

THÈSE PRÉSENTÉE  
POUR OBTENIR LE GRADE DE  
**DOCTEUR**  
**DE L'UNIVERSITÉ DE BORDEAUX**  
ECOLE DOCTORALE SCIENCES PHYSIQUES ET DE  
L'INGÉNIEUR  
LASERS, MATIÈRE, NANOSCIENCES

Par **Maxime Lavaud**

Confined Brownian Motion

Sous la direction de : **Thomas Salez**  
Co-directrion : **Yacine Amarouchene**

Soutenue le 25 décembre 2019

Membres du jury :

Mme. Aude ALPHA	Directrice de Recherche	Université	Rapporteur
M. Bernard BETA	Directeur de Recherche	Université	Rapporteur
M. Georges GAMMA	Directeur de Recherche	Université	Président
Mme. Dominique DELTA	Chargée de Recherche	Université	Examinateuse
M. Eric EPSILON	Ingénieur de Recherche	Université	Examinateur
Mme. Jane DOE	Directrice de Recherche	Université	Directrice
Mme. Simone UNTEL	Ingénieure de Recherche	Université	Invitée

## Abstract

Lorem ipsum dolor sit amet, consectetuer adipiscing elit. Ut purus elit, vestibulum ut, placerat ac, adipiscing vitae, felis. Curabitur dictum gravida mauris. Nam arcu libero, nonummy eget, consectetuer id, vulputate a, magna. Donec vehicula augue eu neque. Pellentesque habitant morbi tristique senectus et netus et malesuada fames ac turpis egestas. Mauris ut leo. Cras viverra metus rhoncus sem. Nulla et lectus vestibulum urna fringilla ultrices. Phasellus eu tellus sit amet tortor gravida placerat. Integer sapien est, iaculis in, pretium quis, viverra ac, nunc. Praesent eget sem vel leo ultrices bibendum. Aenean faucibus. Morbi dolor nulla, malesuada eu, pulvinar at, mollis ac, nulla. Curabitur auctor semper nulla. Donec varius orci eget risus. Duis nibh mi, congue eu, accumsan eleifend, sagittis quis, diam. Duis eget orci sit amet orci dignissim rutrum.

# Table of Contents

<b>Abstract</b>	i
<b>Table of Contents</b>	ii
<b>List of Figures</b>	iv
<b>Nomenclature</b>	v
<b>List of Abbreviations</b>	vi
<b>1 Brownian motion</b>	1
1.1 The Brownian motion discovery . . . . .	1
1.2 Einstein's Brownian theory . . . . .	2
1.3 The Langevin Equation . . . . .	6
1.4 Numerical simulation of bulk Brownian motion . . . . .	11
1.4.1 The numerical Langevin Equation . . . . .	11
1.4.2 Simulating Brownian motion using Python . . . . .	13
1.4.3 Speedup using Cython . . . . .	16
1.5 Conclusion . . . . .	17
<b>2 Stochastic inference of surface-induced effects using Brownian motion</b>	18
2.1 Confined Brownian motion theory . . . . .	18
2.1.1 Gravitational interactions . . . . .	19
2.1.2 Sphere-wall interactions . . . . .	20
2.1.3 Local diffusion coefficient . . . . .	28
2.1.4 Langevin equation for the confined Brownian motion . . . . .	34
2.1.5 Spurious drift . . . . .	34
2.1.6 Numerical simulation of confined Brownian motion . . . . .	35
2.2 Experimental study . . . . .	35
2.2.1 MSD . . . . .	35
2.2.2 Non-gaussian dynamics - Displacement distribution . . . . .	35
2.2.3 Local diffusion coefficient inference . . . . .	35
2.2.4 Precise potential inference using multi-fitting technique . . . . .	35
2.2.5 Measuring external forces using the local drifts . . . . .	35
2.3 conclusion . . . . .	35
<b>References</b>	36

# List of Figures

Fig. 1:	Brownian motion of $1 \mu\text{m}$ particles in water tracked by hand by Jean Perrin and his colleagues. The points are spaced in time by 30 seconds and 16 divisions represents $50 \mu\text{m}$ .	2
Fig. 2:	Simulation of the bulk Brownian motion of $1 \mu\text{m}$ particles in water. On the top each line represents the trajectory of a Brownian particle over 100 seconds. A total of 100 trajectories or shown. On the bottom, bullets represents the Mean Square Displacement (MSD) computed from the simulated trajectories. The black plain line represents Einstein's theory, which is computed from the square of Eq.1.2.11.?	5
Fig. 3:	Bullets represents the probability density function of $w_i$ , a Gaussian distributed number with a mean value $\langle w_i \rangle$ and a variance $\langle w_i^2 \rangle = \tau$ . The plain black line represents a gaussian of zero mean and a $\tau$ variance, Eq.1.4.3. On the first line simulation is done with $\tau = 10^{-3} \text{ s}$ and $\tau = 1 \text{ s}$ on the second one. Each column correspond to a number of draw $N$ , from the left to the right $N = 10^2, 10^3$ and $10^4$ .	11
Fig. 4:	Mean Relative Squared Error (MRSE) of the PDF measured from a generation of $N$ Gaussian random number $w_i$ , and, the actual Gaussian over which the generation is done, Eq.1.4.3. The generation is done over a Gaussian which has a mean value $\langle w_i \rangle = 0$ and the variance $\langle w_i^2 \rangle = \tau$ . We explore generation ranging from $N = 10$ to $10^7$ and $\tau = 10^{-2}$ to $10 \text{ s}$	13
Fig. 5:	a) Set of 100 trajectories simulated using the full Langevin equation for particle of a radius $a = 1 \mu\text{m}$ and a mass $m = 10 \mu\text{g}$ in water, $\eta = 0.001 \text{ Pa.s}$ . The simulations are done with a time step $\tau = 0.01 \text{ s}$ . b) Bullets represents the measured Mean Squared Displacement (MSD) of the simulated trajectories. The plain black line represents the characteristic time of the diffusion, here $\tau_B = m/\gamma = 0.53 \text{ s}$ . The dotted line represents the MSD theory when $t \ll \tau_B$ , $\text{MSD} = \tau^2 k_B T/m$ . The dashed line when $t \gg \tau_B$ , $\text{MSD} = 2D\tau$ . A detailed explanation of the simulation process can be found in the appendix.??.	16
Fig. 6:	Experimental trajectory of a particle of polystyrene of radius $a = 1.5 \mu\text{m}$ near a wall ( $z = 0$ ) along the $z$ axis — perpendicular to the wall.	18
Fig. 7:	A Brownian colloid diffusing near a wall. Both wall and colloid's surface charge negatively, in consequence, a layer of positively charged ions are towards the surfaces, forming a double-layer charge distribution.	21

---

Fig. 8:	A colloid of radius $a$ separated from a wall from a distance $z$ . The colloid material has a static dielectric constant $\epsilon_1$ , the wall $\epsilon_2$ and the solution $\epsilon_3$ .	25
Fig. 9:	a) Potential energy of a colloid of Boltzmann length $\ell_B = 500$ nm. The electrostatic potential $U_{\text{elec}}$ is here characterized by a surface charge constant $B = 4 k_B T$ and a Debye length $\ell_D = 50$ nm. b) Corresponding Gibbs-Boltzmann equilibrium distribution of position.	28
Fig. 10:	Figure extracted from [13], on the left is the experimental setup used. It is an inverted microscope used in order to track particle of size $2R$ inside a cell of thickness $t$ . On the right is their final result, where they measure the diffusion parallel coefficient $D_\perp$ given by Eq.2.1.41, here normalized by $D_0$ the bulk diffusion coefficient as a function of $\gamma$ a confinement constant $\gamma = (\langle z \rangle - a)/a$ .	29
Fig. 11:	Schematic representation of a spherical colloid moving near a wall and the induced shear rate $\dot{\gamma}$ .	31
Fig. 12:	a) Parallel and perpendicular hindered relative diffusion coefficient for a colloidal particle of radius $a = 1.5 \mu\text{m}$ . b) Perpendicular hindered relative diffusion coefficient for a colloid particle of radius $a = 1.5\mu\text{m}$ . In black the exact solution given by the infinite sum Eq.2.1.40. In green the Padé approximation, Eq.2.1.42 and in blue the near wall regime Eq.2.1.43. c) Relative error of the perpendicular hindered coefficient.	33

## Nomenclature

$\alpha$	Noise amplitude
$\ell_B$	Boltzmann length
$\ell_D$	Debye length
$\eta$	Fluid viscosity
$\eta_{\perp}$	Viscosity orthogonal to a wall, see Eq.2.1.40
$\eta_{\parallel}$	Viscosity parallel to a wall, see Eq.2.1.41
$\gamma$	Friction coefficient
$\rho_F$	Fluid density
$\rho_P$	Particle density
$B$	Amplitude of the electrostatic interactions
$D$	Diffusion coefficient, see Eq.1.2.12
$g$	Gravity constant
$k_B$	Boltzmann Constant
$m$	Mass of a particle
$N_A$	Avogadro constant
$R$	Gas constant
$T$	Temperature
$V_t$	Velocity of a particle
$X_t$	Particle position, see Eq.1.3.19

## List of Abbreviations

<b>fps</b>	Frames per second
<b>MRSE</b>	Mean Relative Squared Error
<b>MSD</b>	Mean Squared Displacement
<b>PDF</b>	Probability Density Function
<b>RICM</b>	Reflection Interference Contrast Microscopy
<b>SDE</b>	Stochastic Differential Equations

# 1 Brownian motion

## 1.1 The Brownian motion discovery

In 1827 the Scottish botanist Robert Brown published an article [25] on his observation on the pollen of *Clarkia pulchella* with a lot of details on his thought processes. His experiments were made to understand the flower reproduction, but, as he was looking through the microscope he observed some minute particles ejected from the pollen grains. At first, he thought the goal of this movement was to test the presence of a male organ. In order to test this theory, he extended his observations to Mosses and *Equiseta*, which were drying for a hundred years. However, the fact that this peculiar movement was still observable made him invalidate his theory. Interestingly each time that he encountered a material that he was able to reduce to a fine enough powder to be suspended in water, he observed the same type of motion, although, he never understood its particle's movement.

The difficulty at this time to observe and capture such a movement made the study of what we call today Brownian motion quite difficult and the first theoretical work was actually done by Louis Bachelier in his PhD thesis “The theory of speculation”, where he described a stochastic analysis of the stock and option market. Nowadays, the mathematical description of random movement is still used in the modern financial industry.

It is finally in 1905 that Albert Einstein theoretically state that “bodies of microscopically visible size suspended in a liquid will perform movements of such a magnitude that they can be easily observed in a microscope” [4]. A remark to make here is that in 1948 Einstein wrote a letter to one of his friend where he stated having deduced the Brownian motion “from mechanics, without knowing that anyone had already observed anything of the kind” [26].

It is in 1908 that Jean Perrin published his experimental work on Brownian motion. that way he was able to measure the Avogadro number and prove the kinetic theory that Einstein developed. I would also cite Chaudesaigues and Dabrowski, who helped Perrin to track the particles by hand, half-minutes by half-minutes, for more than 3000 displacements (25 hours) and several particles. This impressive and daunting work is highly detailed in “*Mouvement brownien et molécules*” [27]. This is partly due the results this work that Perrin received the Nobel award in 1926.

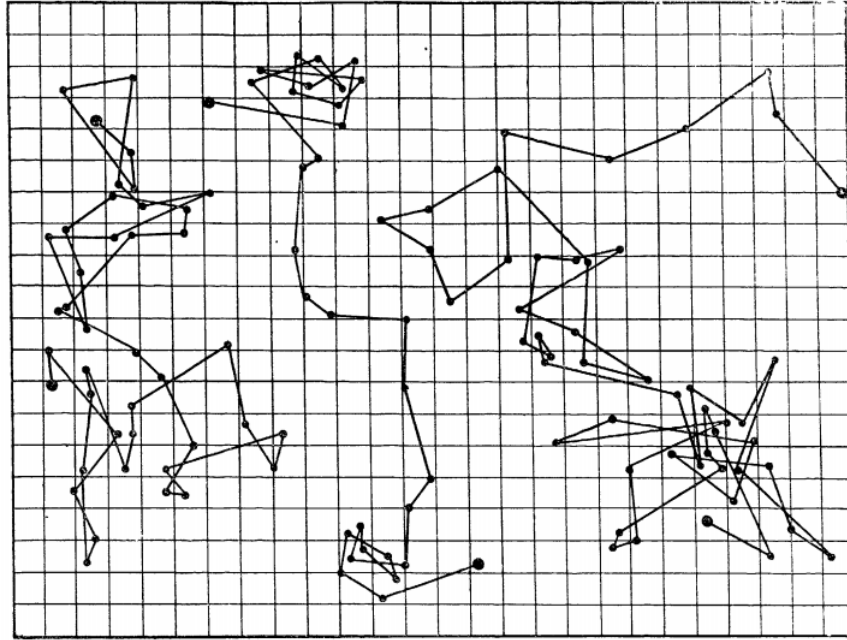


Figure 1: Brownian motion of  $1 \mu\text{m}$  particles in water tracked by hand by Jean Perrin and his colleagues. The points are spaced in time by 30 seconds and 16 divisions represents  $50 \mu\text{m}$ .

## 1.2 Einstein's Brownian theory

In this section we will derive the main characteristics of bulk Brownian motion in the manner of Einstein in 1905 by summarizing the section 4 of [4]. We will then examine the random motion of particles suspended in a liquid and its relation to diffusion, caused by thermal molecular motion. We assume that each particle motion is independent of other particles; also the motions of one particle at different times are assumed to be independent of one another provided that the time interval is not too small. Furthermore, we now introduce a time interval  $\tau$  which is small compared to the observation time but large enough so that the displacements in two consecutive time intervals  $\tau$  may be taken as independent events.

For simplicity, we will here look only at the Brownian motion of  $n$  particles in 1D along the  $x$  axis. In a time interval  $\tau$  the position of each individual particle will increase by a displacement  $\Delta$ , positive or negative. The number of particles  $dn$  experiencing a displacement lying between  $\Delta$  and  $\Delta + d\Delta$  in a time interval  $\tau$  is written as:

$$dn = n\varphi(\Delta)d\Delta , \quad (1.2.1)$$

where

$$\int_{-\infty}^{\infty} \varphi(\Delta) d\Delta = 1 , \quad (1.2.2)$$

and  $\varphi$  is the probability distribution of displacement. We assume for now, that  $\varphi$  is a Gaussian distribution, with a variance scaling linearly with  $\tau$ . Additionally, since such a distribution is even, it satisfies:  $\varphi(\Delta) = \varphi(-\Delta)$ .

Let  $f(x, t)$  be the number of particles per unit volume. From the definition of the function  $\varphi(\Delta)$  we can obtain the distribution of particles found at time  $t + \tau$  from their distribution at a time  $t$ , through:

$$f(x, t + \tau) = \int_{-\infty}^{+\infty} f(x - \Delta, t) \varphi(\Delta) d\Delta . \quad (1.2.3)$$

Since we suppose that  $\tau$  is very small with respect to  $t$ , we have at first order in time:

$$f(x, t + \tau) \simeq f(x, t) + \tau \frac{\partial f}{\partial t} . \quad (1.2.4)$$

Besides, we can Taylor expand  $f(x + \Delta, t)$  in powers of  $\Delta$  since only small values of  $\Delta$  contribute. We obtain:

$$f(x - \Delta, t) = f(x, t) - \Delta \frac{\partial f(x, t)}{\partial x} + \frac{\Delta^2}{2!} \frac{\partial^2 f(x, t)}{\partial x^2} . \quad (1.2.5)$$

Combining Eqs. 1.2.4, 1.2.5 and 1.2.3 we obtain:

$$f + \frac{\partial f}{\partial t} \tau = f \int_{-\infty}^{+\infty} \varphi(\Delta) d\Delta + \frac{\partial f}{\partial x} \int_{-\infty}^{+\infty} \Delta \varphi(\Delta) d\Delta + \frac{\partial^2 f}{\partial x^2} \int_{-\infty}^{+\infty} \frac{\Delta^2}{2} \varphi(\Delta) d\Delta . \quad (1.2.6)$$

On the right-hand side, since  $\varphi(x)$  is an even function, the second term vanishes. Taking into account Eq. 1.2.2 and invoking the definition:

$$\frac{1}{\tau} \int_{-\infty}^{+\infty} \frac{\Delta^2}{2} \varphi(\Delta) d\Delta = D , \quad (1.2.7)$$

Eq.1.2.6 finally becomes:

$$\frac{\partial f}{\partial t} = D \frac{\partial^2 f}{\partial x^2}. \quad (1.2.8)$$

We can here recognize a partial equation of diffusion with  $D$  the diffusion coefficient. We will now initiate the same position  $x = 0$  for all the particles at  $t = 0$  as in Fig.2.  $f(x, t)dx$  denotes the number of particles whose positions have increased between the times 0 and  $t$  by a quantity lying between  $x$  and  $x + dx$  such that we must have:

$$f(x \neq 0, t = 0) = 0 \text{ and } \int_{-\infty}^{+\infty} f(x, t)dx = n. \quad (1.2.9)$$

The solution Eq.1.2.8 is then the Green's function of the heat equation in the bulk:

$$f(x, t) = \frac{1}{\sqrt{4\pi D}} \frac{\exp\left(\frac{-x^2}{4Dt}\right)}{\sqrt{t}}. \quad (1.2.10)$$

From this solution we can see that the mean value of the displacement along the  $x$  axis is equal to 0 and the square root of the arithmetic mean of the squares of displacements (that we commonly call the Root Mean Square Displacement (RMSD)) is given by:

$$\lambda_x = \sqrt{\langle \Delta^2 \rangle} = \sqrt{2Dt}. \quad (1.2.11)$$

The mean displacement is thus proportional to the square root of time. This result is generally the first behavior that we check when we study Brownian motion. In 3D, the square root of the MSD will be given by  $\lambda_x\sqrt{3}$ .

Previously in his article [4], Einstein had found by writing the thermodynamic equilibrium of a suspension of particles that the diffusion coefficient of a particle should read:

$$D = \frac{RT}{N_A} \frac{1}{6\pi\eta a} = \frac{k_B T}{6\pi\eta a}, \quad (1.2.12)$$

with  $R$  the gas constant,  $T$  the temperature,  $N_A$  the Avogadro number,  $\eta$  the fluid viscosity and  $k_B$  the Boltzmann constant. Thus, an experimental measurement of  $D$  could lead to a measurement of the Avogadro number since:

$$N_A = \frac{t}{\lambda_x^2} \frac{RT}{3\pi\eta a} . \quad (1.2.13)$$

Furthermore, measuring  $N_A$  also gives us the mass of atoms and molecules since the mass of a mole is known; as an example the mass of an oxygen atom will be given by  $\frac{16}{N_A}$  and the mass a water molecule by  $\frac{18}{N_A}$ . Finally, Einstein ends up in article [4] by writing “*Let us hope that a researcher will soon succeed in solving the problem posed here, which is of such importance in the theory of heat!*”. I would like here to emphasize the importance of solving this problem at the very beginning of the 20th century. At this time two theories about the fundamental matter components existed, one involving energy and a continuum description in terms of field, and the other one, discrete atoms, especially supported by Boltzmann and his kinetic theory of gases, used by Einstein. Due to a lot of theoretical misunderstandings and experimental error scientist such as Svedberg or Henri thought that Einstein’s theory was false [28] by even suggesting that the statistical properties of Brownian motion were changing with the pH of the solution. It is finally in 1908 that Chaudesaigues and Perrin published all the evidence to prove Einstein’s theory mainly by their ability to create particle emulsions of well controlled radii.

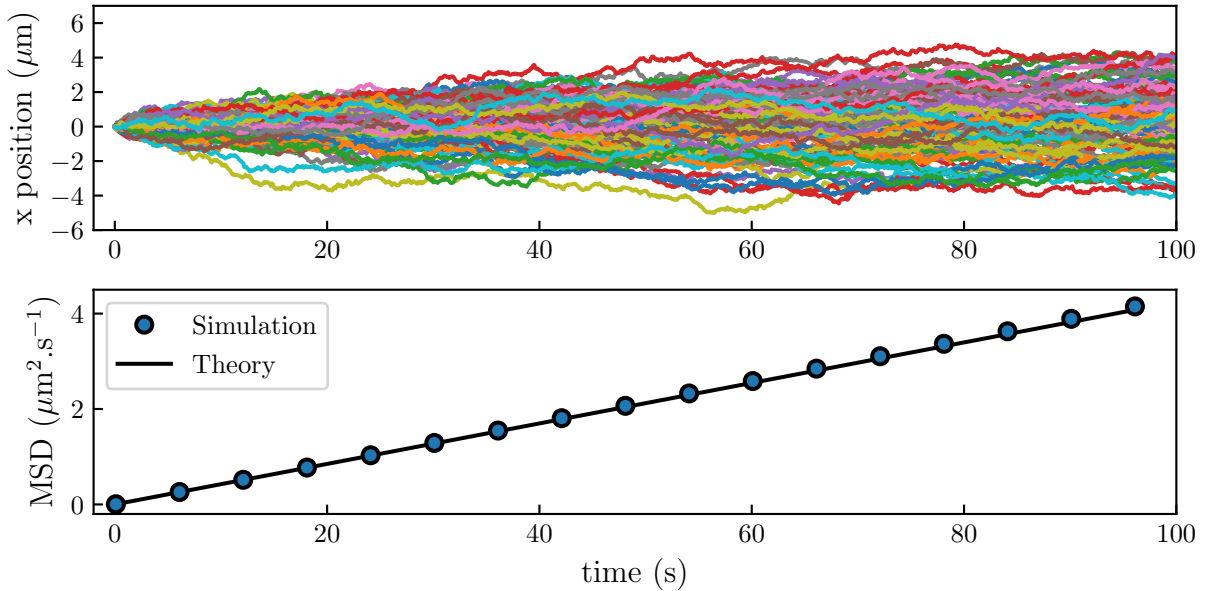


Figure 2: Simulation of the bulk Brownian motion of  $1 \mu\text{m}$  particles in water. On the top each line represents the trajectory of a Brownian particle over 100 seconds. A total of 100 trajectories are shown. On the bottom, bullets represent the Mean Square Displacement (MSD) computed from the simulated trajectories. The black plain line represents Einstein’s theory, which is computed from the square of Eq.1.2.11.  $\clubsuit$

### 1.3 The Langevin Equation

In physics we generally describe Brownian motion through a particular Stochastic Differential Equations (SDE). This model was introduced in 1908 by Langevin [29], this model is now used by the major part of physicists working on random processes. The Langevin equation for a free colloid reads:

$$m dV_t = -\gamma V_t dt + \alpha dB_t , \quad (1.3.1)$$

with  $m$  the mass and  $V_t$  the velocity of the particle. This SDE is the Newton's second law, relating the particle momentum change on the left-hand side of the equation to forces on the right-hand side. We see that the total force applied on the particle is given by two terms: a friction term, with a Stokes-like fluid friction coefficient  $\gamma$ , a random force with  $\alpha$  that we will detail for a spherical particle,  $dB_t$  a random noise which has a Gaussian distribution of zero mean thus:

$$\langle dB_t \rangle = 0 , \quad (1.3.2)$$

and variance equal to:

$$\langle dB_t^2 \rangle = dt . \quad (1.3.3)$$

For a spherical particle the friction term is given by the Stoke's formula:  $\gamma = 6\pi\eta a$  with  $\eta$  the fluid viscosity and  $a$  the particle radius. Thus, we can derive the mean value of the particle velocity as:

$$\langle \frac{dV_t}{dt} \rangle = -\frac{\gamma}{m} \langle V_t \rangle dt + \frac{\alpha}{m} \langle dB_t \rangle , \quad (1.3.4)$$

with the properties of  $dB_t$  given by Eq.1.3.2, it becomes:

$$\langle dV_t \rangle = -\frac{\gamma}{m} \langle V_t \rangle dt . \quad (1.3.5)$$

Moreover, without a loss of generality, the average of a variable  $x$ ,  $\langle x \rangle$ , is done over a set

of  $N$  observations  $\{x_i\}$  such as:

$$\langle x \rangle = \frac{1}{N} \sum_{i=1}^N x_i , \quad (1.3.6)$$

one can then show that:

$$\frac{d}{dt} \langle x \rangle = \frac{d}{dt} \left[ \frac{1}{N} \sum_{i=1}^N x_i \right] = \frac{1}{N} \sum_{i=1}^N \frac{d}{dt} x_i = \langle \frac{d}{dt} x \rangle . \quad (1.3.7)$$

The latter thus shows that it is possible to invert average value  $\langle \cdot \rangle$  and a derivative. Therefor, Eq.1.3.5 becomes:

$$\frac{d}{dt} \langle V_t \rangle = -\frac{\gamma}{m} \langle V_t \rangle , \quad (1.3.8)$$

which has a familiar solution:

$$\langle V_t(t) \rangle = V_0 e^{-\frac{\gamma}{m} t} , \quad (1.3.9)$$

with  $V_0$  an initial velocity. This result shows that the average of the velocity should decay to zero with a characteristic time  $\tau_B = \frac{m}{\gamma}$ . For instance, the polystyrene particles used during my experiments which are micro-metric we have  $\tau_B \approx 10^{-7}$  s. This means that if we measure the displacements of a particle with a time interval  $\tau \gg \tau_B$  the displacement can be taken as independent events as it was stated by Einstein. In physical terms, this means that we are in the over-damped regime, in this case the Langevin equation reads:

$$-\gamma V_t dt + \alpha dB_t = 0 . \quad (1.3.10)$$

The experiments done during my thesis used a video camera that can reach a maximum of hundreds frames per second (fps) reaching time steps of  $\approx 10^{-2}$  s. Therefore, all my work falls into the over damped regime. Before focusing definitely on Eq.1.3.10, we can use Eq.1.3.4 to characterize further the unknown coefficient  $\alpha$ . In order to do so we compute the mean square value of Eq.1.3.4, starting by taking the second order Taylor expansion:

$$\begin{aligned} d(V_t^2) &\simeq \frac{\partial V_t^2}{\partial V_t} dV_t + \frac{1}{2} \frac{\partial^2 V_t^2}{\partial V_t^2} (dV_t)^2 \\ &= 2V_t dV_t + (dV_t)^2 \end{aligned} \quad (1.3.11)$$

combining Eqs.1.3.1 and 1.3.11, we obtain by only keeping the terms of order  $dt$ :

$$d(V_t^2) = 2V_t \left( -\frac{\gamma}{m} V_t dt + \frac{\alpha}{m} dB_t \right) + \frac{\alpha^2}{m^2} dB_t^2 . \quad (1.3.12)$$

Thus, the average value of  $d(V_t^2)$  reads:

$$\langle d(V_t^2) \rangle = -2\frac{\gamma}{m} \langle V_t^2 \rangle dt + 2\frac{\alpha}{m} \langle V_t dB_t \rangle + \frac{\alpha^2}{m^2} \langle dB_t^2 \rangle . \quad (1.3.13)$$

Moreover, since  $dB_t$  is chosen independently of the velocity  $V_t$ , one can write  $\langle V_t dB_t \rangle = \langle V_t \rangle \langle dB_t \rangle = 0$ . Taking the latter remark into account and the fact that  $\langle dB_t^2 \rangle = dt$ , Eq.1.3.13 becomes:

$$\langle d(V_t^2) \rangle = \left[ -2\frac{\gamma}{m} \langle V_t^2 \rangle + \frac{\alpha^2}{m^2} \right] dt . \quad (1.3.14)$$

Since equilibrium averages in thermodynamics must become time independent, we have  $\langle d(V_t^2) \rangle = 0$ , thus:

$$\langle V_t^2 \rangle = \frac{\alpha^2}{2\gamma m} . \quad (1.3.15)$$

Besides, from the equipartition of energy we also know that:

$$\langle \frac{1}{2} m V_t^2 \rangle = \frac{1}{2} k_B T . \quad (1.3.16)$$

The latter equation permits a direct determination of the amplitude of the noise  $\alpha$ :

$$\alpha = \sqrt{2k_B T \gamma} . \quad (1.3.17)$$

The latter result permits to compute the amplitude of the random force in the Langevin equation. Taking the over-damped Langevin equation, it reads:

$$V_t dt = \sqrt{2 \frac{k_B T}{\gamma}} dB_t \quad (1.3.18)$$

Furthermore, one can write the position of the particule  $X_t$  at a time  $t$ , such as:

$$X_t = \int_0^t V_{t'} dt' , \quad (1.3.19)$$

where we can suppose at the initial time  $t = 0$  that  $X_0 = 0$ . Computing  $\langle X_t^2 \rangle$  using Eqs.1.3.18,1.3.19 and 1.3.3 thus gives:

$$\langle X_t^2 \rangle = 2 \frac{k_B T}{\gamma} t = 2 D t \quad (1.3.20)$$

By relating  $\langle X_t^2 \rangle$  to the Mean Square Displacement (MSD) to the initial position such as:

$$\text{MSD} = \langle (X_0 - X_t)^2 \rangle = \langle X_t^2 \rangle , \quad (1.3.21)$$

we obtain that the MSD should be linear with the time. This result confirms that using the over-damped Langevin equation, leads to the Einstein's result Eq.1.2.11. Where one can identify the diffusion coefficient of the particle to be  $D = k_B T / \gamma$ . Additionally, the latter identity is called the Stokes-Einstein relation.

Additionally, the Langevin equation is great to compute correlator such as the velocity correlator  $\langle V_t V_{t''} \rangle$  which the simplest to compute and the one that we will detail below. Indeed, if we use the full Langevin equation,  $\langle X_t^2 \rangle$  can't be that easily computed since  $m dV_t$  does not vanish. We would thus need to rewrite Eq.1.3.20 using the velocity correletor such as:

$$\langle X_t^2 \rangle = \int_0^t \int_0^t \langle V_{t'} V_{t''} \rangle dt' dt'' . \quad (1.3.22)$$

Let us now study how the two-point correlator function  $\langle V_t V_{t''} \rangle$ , using the full Langevin

equation multiplied by  $V_0$  and following the same steps as for Eq.1.3.9, one has:

$$\langle V_t V_0 \rangle = \langle V_0^2 \rangle e^{-t/\tau_B} . \quad (1.3.23)$$

As the equilibrium state is invariant under temporal translation and assuming that  $V_0$  has an equilibrium steady-state distribution with  $\langle V_0^2 \rangle = k_B T / m$  we have:

$$\langle V_t V'_t \rangle = \frac{k_B T}{m} e^{-|t-t'|/\tau_B} . \quad (1.3.24)$$

One can solve Eq.1.3.22 by splitting the integral in two parts, where  $t' > t''$  and  $t' < t''$ :

$$\begin{aligned} \langle X_t^2 \rangle &= \frac{k_B T}{m} \int_0^t dt' \int_0^{t'} dt'' e^{-|t'-t''|/\tau_B} = 2 \frac{k_B T}{\gamma} \left( \int_0^t dt' \left[ 1 - e^{-t'/\tau_B} \right] \right) \\ &= 2 \frac{k_B T}{\gamma} \left( t - \tau_B \left[ 1 - e^{-t/\tau_B} \right] \right) . \end{aligned} \quad (1.3.25)$$

We can extract two results from that equation. At short time  $t \ll \tau_B$ , one has:

$$\begin{aligned} \langle X_t^2 \rangle &\simeq 2 \frac{k_B T}{\gamma} \left( t - \tau_B \left[ 1 - 1 + \frac{t}{\tau_B} - \frac{t^2}{2\tau_B^2} \right] \right) \\ &= \frac{k_B T}{m} t^2 . \end{aligned} \quad (1.3.26)$$

This is the ballistic regime. If one can experimentally explore times shorter than  $\tau_B$  one will then measure the real velocity of the particle. At longer times,  $t \gg \tau_B$ , the MSD is given by:

$$\langle X_t^2 \rangle \simeq 2 \frac{k_B T}{\gamma} t = 2 D t . \quad (1.3.27)$$

This is the diffusive regime where the MSD, as found earlier, Eq.1.3.20 with the over-damped Langevin equation. To study this different results, it can be interesting to simulate the Brownian motion.

## 1.4 Numerical simulation of bulk Brownian motion

### 1.4.1 The numerical Langevin Equation

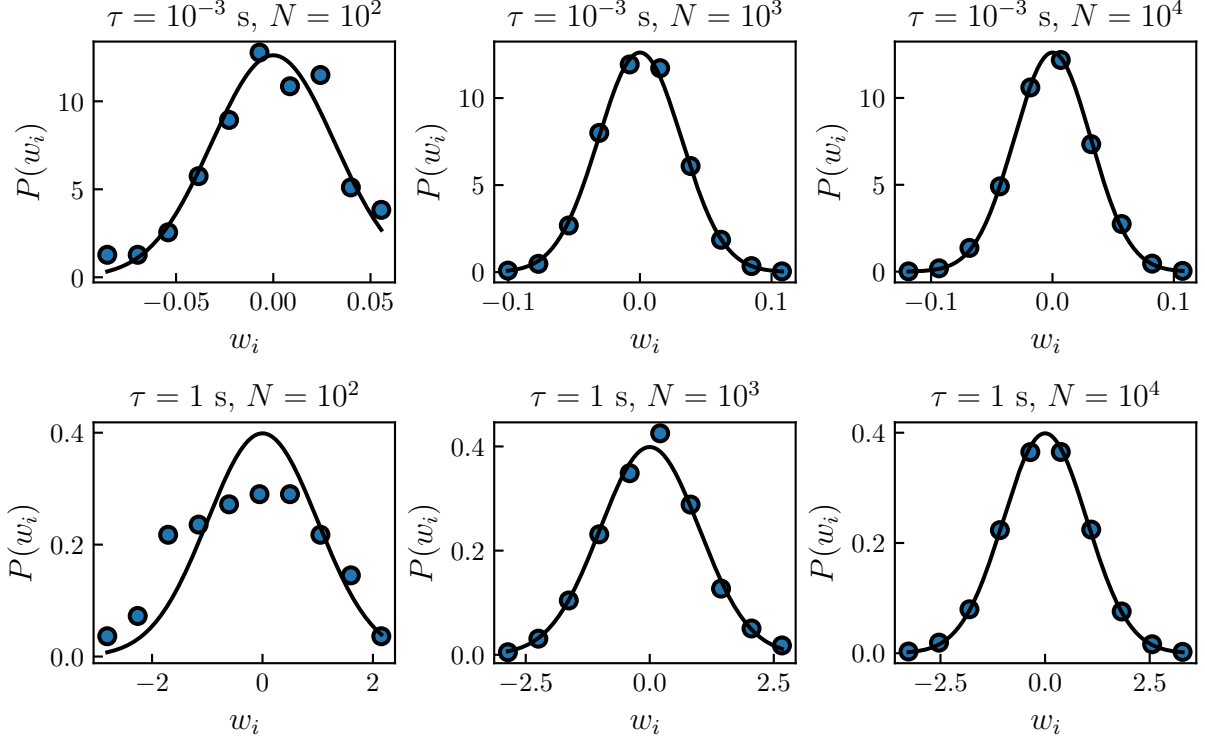


Figure 3: Bullets represents the probability density function of  $w_i$ , a Gaussian distributed number with a mean value  $\langle w_i \rangle$  and a variance  $\langle w_i^2 \rangle = \tau$ . The plain black line represents a gaussian of zero mean and a  $\tau$  variance, Eq.1.4.3. On the first line simulation is done with  $\tau = 10^{-3}$  s and  $\tau = 1$  s on the second one. Each column correspond to a number of draw  $N$ , from the left to the right  $N = 10^2$ ,  $10^3$  and  $10^4$ .

The Langevin equation is an ordinary differential equation that can easily be numerically simulated in the bulk case. If one approximate the continuous position of a particle  $X_t$  at a time  $t$  by a discrete-time sequence  $x_i$  which is the solution of the equation at a time  $t_i = i\tau$  with  $\tau$  being the time step of the simulation. One can then use the Euler method to numerically write  $V_t$  as

$$V_t \simeq \frac{x_i - x_{i-1}}{\tau} , \quad (1.4.1)$$

and  $dV_t$  as

$$\begin{aligned}\frac{dV_t}{dt} &\simeq \frac{\frac{x_i - x_{i-1}}{\tau} - \frac{x_{i-1} - x_{i-2}}{\tau}}{\tau} \\ &= \frac{x_i - 2x_{i-1} + x_{i-2}}{\tau^2}.\end{aligned}\quad (1.4.2)$$

The only term remaining to be computed numerically is the random term  $dB_t$ . One can thus replace  $dB_t/dt$  by  $w_i$ <sup>1</sup> a Gaussian distributed random number generated with a mean  $\langle w_i \rangle = 0$  and a variance  $\langle w_i^2 \rangle = \tau$ . The Probability Density function (PDF) of the Gaussian distribution is thus given by:

$$P(w_i) = \frac{1}{\sqrt{2\pi\tau}} e^{-\frac{w_i^2}{2\tau}}. \quad (1.4.3)$$

Such a number can be simply generated with the following Python snippet.

---

```

1 import numpy as np
2
3 tau = 0.5 # time step in seconds
4 wi = np.random.normal(0, np.sqrt(tau))

```

---

In the latter, `random.normal()` is a built-in Numpy module that permits the generation of Gaussian distributed random numbers. Finally, by combining Eqs.1.4.1, 1.4.2 and  $w_i$ , the full Langevin equation becomes:

$$m \frac{x_i - 2x_{i-1} + x_{i-2}}{\tau^2} = -\gamma \frac{x_i - x_{i-1}}{\tau} + \sqrt{2k_B T \gamma} w_i. \quad (1.4.4)$$

From the latter, one can write  $x_i$  as:

$$x_i = \frac{2 + \tau/\tau_B}{1 + \tau/\tau_B} x_{i-1} - \frac{1}{1 + \tau/\tau_B} x_{i-2} + \frac{\sqrt{2k_B T \gamma}}{m(1 + \tau/\tau_B)} \tau w_i, \quad (1.4.5)$$

where we can observe that we need two initial condition are needed, the two first positions of the particle. Numerically, those positions could be randomly generated or simply set to 0, if enough statics are generated it will not play much into the results.

---

<sup>1</sup> The notation  $w$  was choose since in mathematical term, a real valued continuous-time stochastic process such as  $dB_t$  is called a Wiener process in honor of Norbert Wiener [30].

### 1.4.2 Simulating Brownian motion using Python

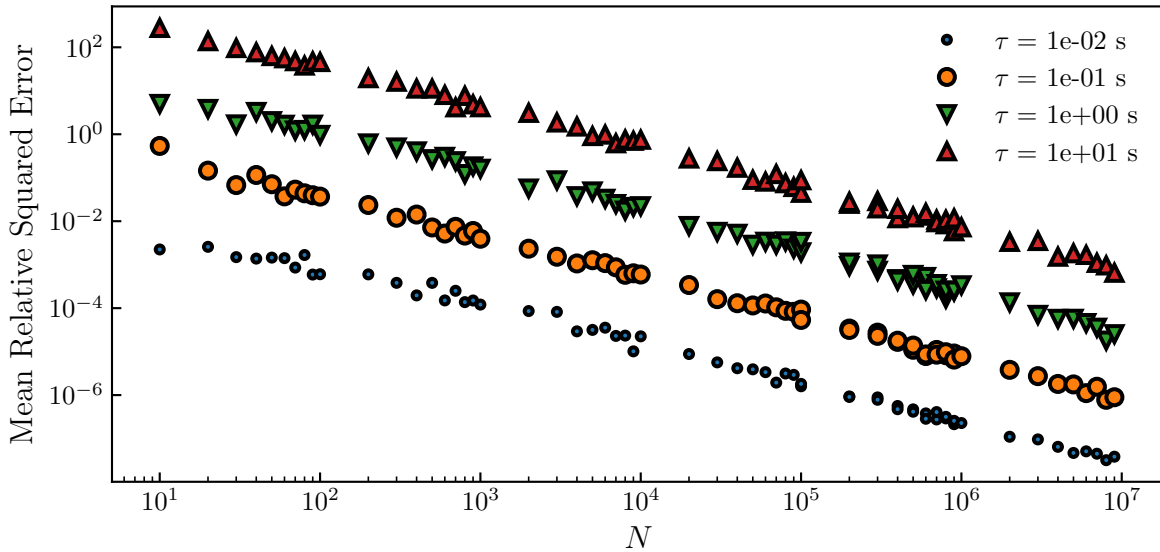


Figure 4: Mean Relative Squared Error (MRSE) of the PDF measured from a generation of  $N$  Gaussian random number  $w_i$ , and, the actual Gaussian over which the generation is done, Eq.1.4.3. The generation is done over a Gaussian which has a mean value  $\langle w_i \rangle = 0$  and the variance  $\langle w_i^2 \rangle = \tau$ . We explore generation ranging from  $N = 10$  to  $10^7$  and  $\tau = 10^{-2}$  to  $10$  s

Before, deeping into the actual simulation, it could be interresting to ask ourselfe about how long the simulation should be. Indeed, for the different observables' mean value to remain constant we should wait a suffisient amount of time. It is possible to have qualitative approach by generating  $N$  number  $w_i$  and measuring the resulting PDF  $P_c(w_i)$  and looking how much we need to increase  $N$  to have  $P_c(w_i) \simeq P(w_i)$ . As we can see on the Fig.3, for simulation made with  $\tau = 10^{-3}$  s and  $\tau = 1$  s, we obervre that as we increase the number of generated numbers  $N$ , the measured PDF, get closer to the real one given by Eq.1.4.3.

To have a more quantitative approach, one can compute the Mean Relative Squared Error (MRSE)) between the measured PDF  $P_c(w_i)$  and  $P(w_i)$  as a function of the number of generated numbers  $N$ , such as:

$$\text{MRSE} = \left\langle \frac{(P_c(w_i) - P(w_i))^2}{P(w_i)^2} \right\rangle_N \quad (1.4.6)$$

where the notation  $|_N$  denotes that  $N$  numbers are generated. Additionaly, since we measure the  $P_c(w_i)$  by doing an histogram, the question of how many bins is used should

be answered. It is possible to use the Freedan-Diaconis rule [31] to compute the width of the bins to be used in a histogram, this rule reads:

$$\text{Bin width} = 2 \frac{\text{IQR}(\{w_i\})}{\sqrt[3]{N}}, \quad (1.4.7)$$

where IQR is the interquartile range, and  $\{w_i\}$  a sample of  $N$  random numbers. Moreover, one should only take 2 bins as a minimum. The actual number of bins can be computed using the following Python snippet.

---

```

1 import numpy as np
2
3 def _iqr(wi):
4     """Function to compute interquartile range."""
5     return np.subtract(*np.percentile(x, [75, 25]))
6
7 def optimal_bins(wi):
8     """
9         Function to compute the optimal number of bins using Freedan-diaconis rule.
10        Input: list of random numbers / Output: optimal bins number
11    """
12
13    n = int(diff(wi) / (2 * _iqr(wi) * np.power(len(wi), -1 / 3)))
14
15    if n <= 2:
16        return 2
17    else:
18        return n

```

---

As we can see on the Fig.4, for  $\tau$  varying between  $10^{-2}$  and 10 seconds, and,  $N$  between 10 and  $10^6$ , the MRSE decreases as  $N$  increases. More over, it is interesting to observe that the MRSE is greater as  $\tau$  increases for a fix  $N$  value. Indeed, as an example we would need to only generate  $N = 10^{-3}$  numbers to obtain a MRSE of  $10^{-4}$  for  $\tau = 0.1$  s, while we would need to  $N = 10^6$  for  $\tau = 1$  s.

Now that the Langevin equation is known numerically, one could use it to simulate some Brownian trajectories. A simple way to do the simulation is shown using Python in the Jupyter notebook framework in the appendix.???. A set of trajectory simulated for a fictive particle of radius  $a = 1 \mu\text{m}$  and mass  $m = 10 \mu\text{g}$  in water is shown in Fig.5-a). For such a particle the diffusive characteristic time is  $\tau_B = 0.53\text{s}$ . Moreover, as one can see on the Fig.5-b), the MSD is correctly modeled by the Eq.1.3.26 for  $\tau \ll \tau_B$  and by the

Eq.1.3.27 for  $\tau \gg \tau_B$ . Please note that for non-continuous data such as the simulation or experimental trajectories, and for a given time increment  $\Delta t$ , the MSD, is generally defined by:

$$\langle \Delta x^2 \rangle|_t = \langle (x(t + \Delta t) - x(t))^2 \rangle|_t , \quad (1.4.8)$$

where the average  $\langle \rangle|_t$  is performed over a time  $t$ . Additionally, it can be numerically using the following Python function.

---

```

1 def msd(x, Dt):
2     """Function that return the MSD for a list of time index Dt for a trajectory x"""
3     _msd = lambda x, t: np.mean((x[:-Dt] - x[Dt:]) ** 2)
4     return [_msd(x, i) for i in t]

```

---

Additionally, as we have seen earlier, the Langevin Equation can be simplified to it's over-damped version Eq.1.3.10. In this case, the time step of the simulation  $\tau$  should be greater than the diffusion time  $\tau_B$ . Thus, one who is interested at the long time statistical properties of the Brownian motion can use the over-damped Langevin equation. In this case by putting  $m = 0$  into Eq.1.4.5, one can write  $x_i$  as:

$$x_i = x_{i-1} + \sqrt{2D}w_i . \quad (1.4.9)$$

The statistical properties at long time could be retrieved by simulating Brownian motion using the full Langevin equation. But, since the integration scheme used for Eq.1.4.5 requires  $\tau \ll \tau_B$  long simulation are necessary to retrieve the over-damped properties. As an example, for the Fig.2 I directly used Eq.1.4.9 for the simulation using the Python Snippet below.

---

```

1 import numpy as np
2
3 N = 1000 # trajectory length
4 D = 1 # diffusion coefficient
5 tau = 0.5 # time step
6 trajectory = np.cumsum(np.sqrt(2 * D) * np.random.normal(0, np.sqrt(tau), N))

```

---

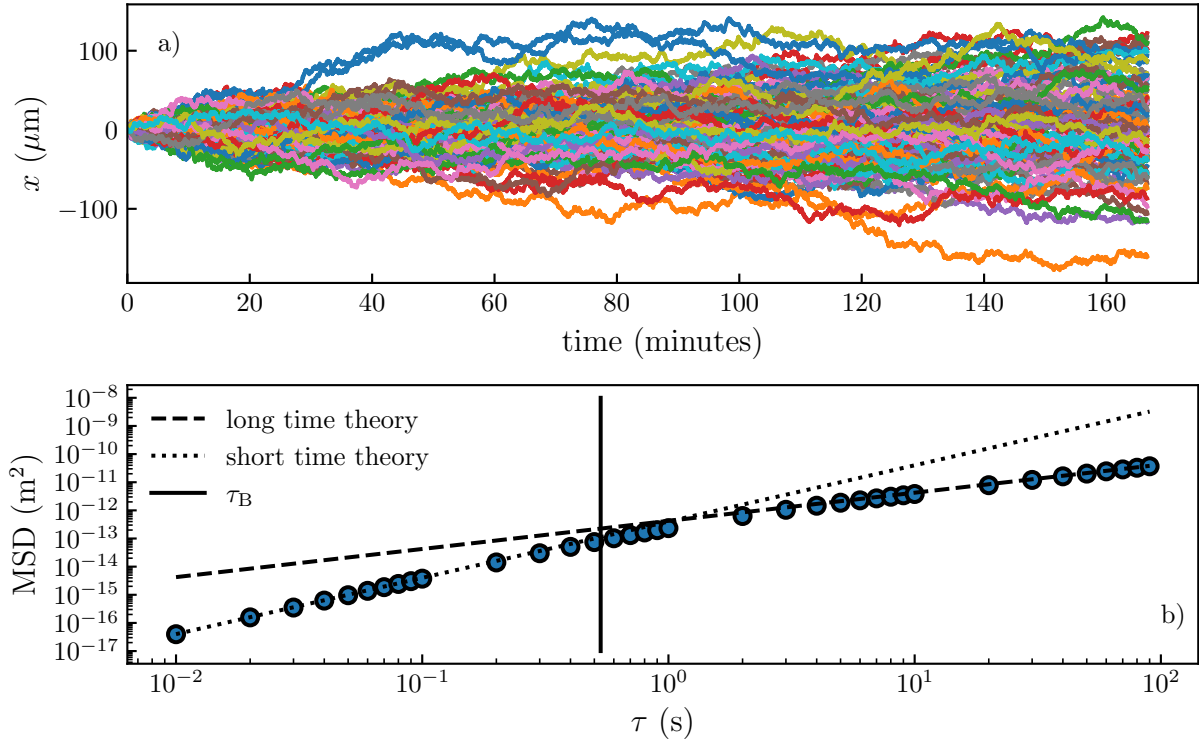


Figure 5: a) Set of 100 trajectories simulated using the full Langevin equation for particle of a radius  $a = 1 \mu\text{m}$  and a mass  $m = 10 \mu\text{g}$  in water,  $\eta = 0.001 \text{ Pa.s}$ . The simulations are done with a time step  $\tau = 0.01 \text{ s}$ . b) Bullets represents the measured Mean Squared Displacement (MSD) of the simulated trajectories. The plain black line represents the characteristic time of the diffusion, here  $\tau_B = m/\gamma = 0.53 \text{ s}$ . The dotted line represents the MSD theory when  $t \ll \tau_B$ ,  $\text{MSD} = \tau^2 k_B T/m$ . The dashed line when  $t \gg \tau_B$ ,  $\text{MSD} = 2D\tau$ . A detailed explanation of the simulation process can be found in the appendix.??.

### 1.4.3 Speedup using Cython

I would like to point out, that the optimization of a simple simulation of Brownian trajectory can be interesting. Indeed, using a pure Python code as presented in the first part of the appendix.??, the simulation of one trajectory of  $10^6$  steps, needs 6 s to be computed. Thus, more than 10 minutes should be required to compute the 100 trajectories showed in the Fig.5. This is long due to how Python always verify that what we do is allowed, it thus needs to verify at each step of the `for` loop the object type of each variable. This is in general the main drawback of the interpreted language, one solution is then to compile the part of the code where the `for` loops are computed. One can use the Cython package in order to specify the type of every single variable, once that done, it will convert the lengthy part in C and compile it. As presented in the appendix.??, doing that on full Langevin simulation reduces the time to generate a  $10^6$  steps trajectory from 6 s to 30 ms thus achieving a speedup of  $\simeq 200\times$ . Moreover, in the compiled version, we are here speed bound by the random number generation, indeed it takes  $24.0 \pm 0.8 \text{ ms}$  using `numpy`.

Additionally, as shown at the end of the appendix.?? even pure C implementation of the random generation can be slower than the `numpy` one, thanks to impressive optimization. Thus, using those tools, this simulation is probably as optimize as it can get.

## 1.5 Conclusion

In this chapter, we have covered the history of the Brownian motion from the first observation of Robert Brown in the middle of 19th century to it's mathematical and experimental proofs in the early 20s. We have then described mathematically the bulk Brownian motion, and its important stastical properties. Finaly, we have used the later description in order to simulate Brownian motion using the both the full Langevin equation and it's over-damped version. In the following chapter, I will describe experimental methods using light interference properties in order to track colloidal particle.

## 2 Stochastic inference of surface-induced effects using Brownian motion

### 2.1 Confined Brownian motion theory

By observing the trajectory along the  $z$  axis of a particle of  $1.5 \mu\text{m}$  as shown on the fig.6, one can see that the particle height does not get higher than  $\simeq 4 \mu\text{m}$ . Indeed due to gravity, the particle is confined near the surface. Brownian motion in confinement and at interfaces is a canonical situation, encountered from fundamental biophysics to nanoscale engineering. This confinement induces near-wall effects, such as hindered mobility and electrostatic interactions.

In the first part of this chapter, I will detail the theory background of the confined Brownian motion and how to numerically simulate it. In a second part, I will present how to analyse experimental data. In particular, I will detail a multi-fitting procedure that allows a thermal-noise-limited inference of diffusion coefficients spatially resolved at the nanoscale, equilibrium potentials, and forces at the femtometer resolution.

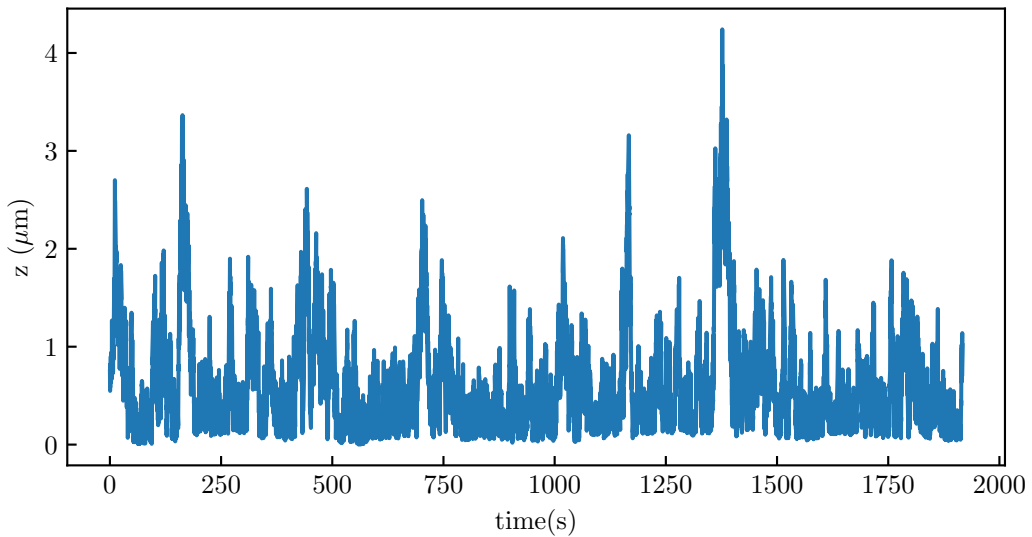


Figure 6: Experimental trajectory of a particle of polystyrene of radius  $a = 1.5 \mu\text{m}$  near a wall ( $z = 0$ ) along the  $z$  axis — perpendicular to the wall.

### 2.1.1 Gravitational interactions

In our experiment, we observe confined Brownian motion since the colloids are subject to gravity. Indeed, the density of the observed colloid  $\rho_p$  is different of the medium  $\rho_m$  — in our experiment water,  $\rho_m = 1000 \text{ kg.m}^{-3}$ . Thus, the particle lies into a gravitational potential given by:

$$U_g(z) = \Delta m g z = \frac{4}{3} \pi a^3 g \Delta \rho z , \quad (2.1.1)$$

where  $\Delta m$  is the mass difference of the particle and a fluid sphere of the same size,  $\Delta \rho$  the corresponding density difference such as  $\Delta \rho = \rho_m - \rho_p$  and  $g$  the gravitational acceleration. By invoking the definition of a distance that we call the Boltzmann length,

$$\ell_B = \frac{k_B T}{4/3 \pi a^3 \Delta \rho g} , \quad (2.1.2)$$

one can rewrite the gravitational potential Eq.2.1.1 as:

$$U_g = \frac{k_B T}{\ell_B} . \quad (2.1.3)$$

The Boltzmann length  $\ell_B$  is the typcal gravitational decay length and represents the balance between the gravitational potential and thermal energy. This distance was first measured by Perrin [5], by enumerating the number of particles as a function of height to reconstruct the concentration of the colloidal suspension that exponentially decays as  $e^{-z/\ell_B}$ . As an exemple, in water, for a particle polystyrene,  $\rho_p = 1050 \text{ kg.m}^{-3}$  and of radius  $a = 1.5 \mu\text{m}$  we have  $\ell_B = 0.58 \mu\text{m}$ .

For particle with  $\ell_B \gg a$ , one can consider that the particle does not feel the gravity. This is particulary the case when the density of the colloids and fluid matches, in this particular case  $\ell_B = 0$ . Thus density matching can be a way to do gravitation free experiments. In the case of our experiment, we want to measure confinement induced effects, therefore, we need this gravitational interaction to have the particles near the surface. Indeed, as a particle gets larger, or, denser  $\ell_B$  decreases and the particle will be, in average, closer to the surface.

### 2.1.2 Sphere-wall interactions

As we have seen, external forces acts on the particle such as the gravity, however it is not the only one. As the Brownian particle is close to a wall we can expect some interactions between the surfaces. In our case, we suppose that the Brownian particles do not interact between each other, which is the case for the dilute solution used. Indeed, the particles studied are at a minimum  $50 \mu\text{m}$  apart which correspond to 10 times their size for the larger beads.

To describes the interaction between, the Brownian particle and the wall, we use the DLVO<sup>2</sup> theory. This theory was first developed to describe the interactions between colloids to explain the stability of colloidal suspension. It describes the interactions using two forces components; the Van Der Waals force which arise form the interactions between surface's molecules and electrostatic interactions due the a double-layer formed with the ions present in the solution.

### Double-Layer interactions

When a surface is immersed in water are usually charged [68] due to a high dielectric constant  $\epsilon \simeq 80$  that permit the build up of charges for low energetic price. Commonly, surface charging is done through ionization of dissociation of surface groups<sup>3</sup>, from the binding of ions from the solution — for example, adsorption of  $-\text{OH}^-$  onto the water-air interface that charge it negatively. In the bulk, a fluid should be electrically neutral, thus the fluid contains as many ions of opposite charge. However, when a surface is charged negatively, negative ions are repelled from the surface, while positive ions are attracted towards the surface. Therefore, a double-layer charge distribution is formed near the surface, as shown Fig.XX. Experimentally, we use glass slides and polystyrene beads, that are both negatively charged in water, thus leading to repulsive double-layer. This repulsive force prevent the colloids to stick together or to the surface of the substrate.

If the solution contains an electrolyte (ions of positive and negative charges), for example a salty solution, containing  $\text{Na}^+$  and  $\text{Cl}^-$  ions. In the DLVO theory, the electrostatic field  $\Psi(\vec{r})$  generated by the double layer satisfies the mean field Poisson's equation [68]:

---

<sup>2</sup> The DLVO theory is named after Derjaguin, Landau, Verwey, and Overbeek [68].

<sup>3</sup> For example, the dissociation of protons from surface carboxylic groups [68] ( $-\text{COOH} \rightarrow -\text{COO}^- + \text{H}^+$ ) which charge negatively the surface.

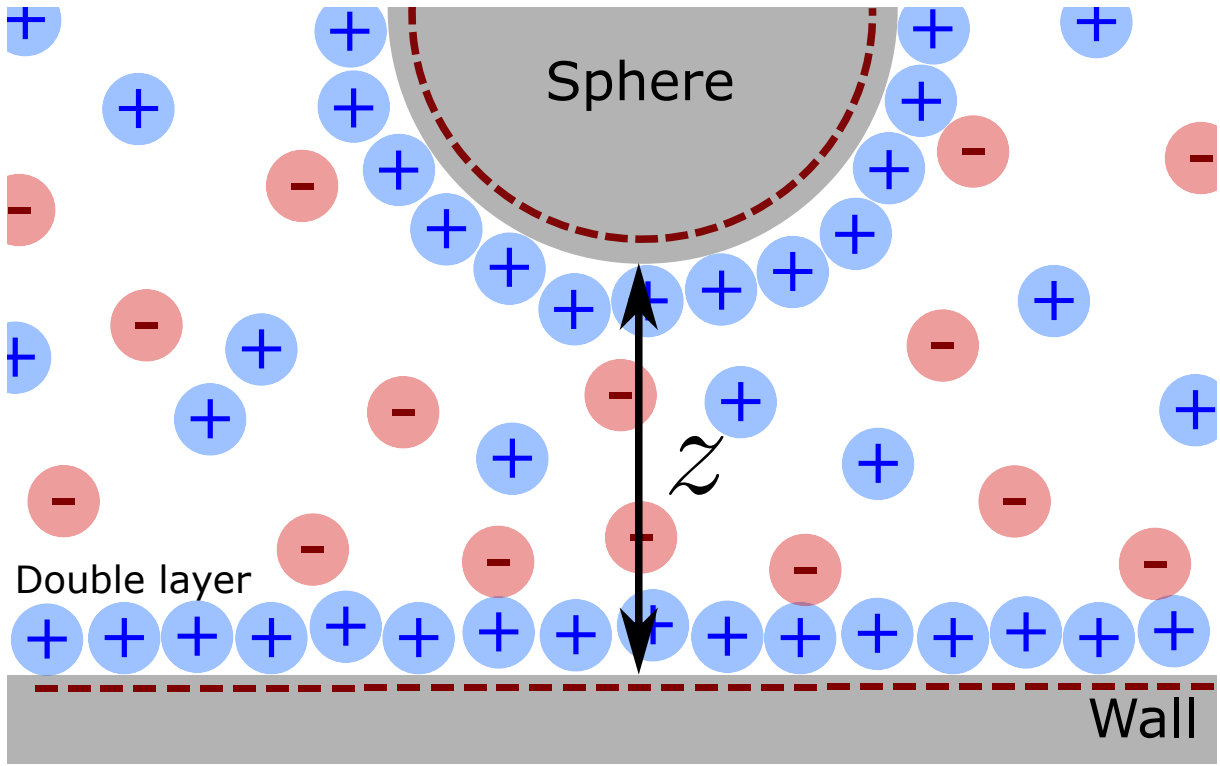


Figure 7: A Brownian colloid diffusing near a wall. Both wall and colloid's surface charge negatively, in consequence, a layer of positively charge ions are towards the surfaces, forming a double-layer charge distribution.

$$\nabla^2 \Psi(\vec{r}) = -\frac{1}{\epsilon_r \epsilon_0} \rho_e(\vec{r}) , \quad (2.1.4)$$

where  $\epsilon_0$  the vacuum permittivity,  $\epsilon_r$  the relative permitivity of the fluid,  $\rho_e(\vec{r})$  the local charge density. The latter can be written as:

$$\rho_e(\vec{r}) = e \sum_i z_i c_i(\vec{r}) , \quad (2.1.5)$$

where  $e$  is the elementary charge,  $i$  denotes an ionic species of valence  $z_i$  and local ionic concentration  $c_i(\vec{r})$  (number density). If the solution is at the thermodynamic equilibrium, the Boltzmann equation is used to calculate the local ion density such that:

$$c_i(\vec{r}) = c_i^0 \exp \left( \frac{z_i e \Psi(\vec{r})}{k_B T} \right) , \quad (2.1.6)$$

where  $c_i^0$  is the bulk concentration (number density) of the ionic species  $i$ . By combining Eqs.2.1.4, 2.1.5 and 2.1.6, one can obtain the Poisson-Boltzmann equation:

$$\nabla^2 \Psi(\vec{r}) = \sum_i \frac{z_i e c_i^0}{\epsilon_0 \epsilon_r} \exp\left(-\frac{z_i e \Psi(\vec{r})}{k_B T}\right) . \quad (2.1.7)$$

Since the Poisson-Boltzmann is non-linear, it is most likely to be solve numerically. However, for simple geometry such as uniformly charged plane or sphere it can be solve analytically. Let consider, to simplify, that we have a monovalent electrolyte, meaning that the electrolyte is composed of two ions of valence equal to one —  $\text{Na}^+$   $\text{Cl}^-$  for example — and  $c_i^0$  is equal to the electrolyte solution concentration  $c_s^0$ . In that case Eq.2.1.7 simplifies to:

$$\begin{aligned} \nabla^2 \Psi(\vec{r}) &= \frac{e c_s^0}{\epsilon_0 \epsilon_r} \left[ \exp\left(\frac{-e \Psi(\vec{r})}{k_B T}\right) - \exp\left(\frac{+e \Psi(\vec{r})}{k_B T}\right) \right] \\ &= 2 \frac{e c_s^0}{\epsilon_0 \epsilon_r} \sinh\left(\frac{e \Psi(\vec{r})}{k_B T}\right) . \end{aligned} \quad (2.1.8)$$

In the case, where the  $\Psi$  is small enough everywhere to have the electrostatic potential energy  $e\Psi \ll k_B T$ , which generally the case when using salty solution. In that case, it is possible, using the a Taylor approximation at the second order to write:

$$\exp\left(-\frac{z_i e \Psi(\vec{r})}{k_B T}\right) \simeq 1 + \frac{z_i e \Psi(\vec{r})}{k_B T} . \quad (2.1.9)$$

Thus, the Poisson-Boltzmann equation (Eq.2.1.7) becomes:

$$\nabla^2 \Psi(\vec{r}) = \sum_i \frac{z_i e c_i^0}{\epsilon_0 \epsilon_r} \left( 1 + \frac{z_i e \Psi(\vec{r})}{k_B T} \right) . \quad (2.1.10)$$

Since the fluid in the bulk, is electrically neutral, the first term vanishes as  $\sum_i z_i c_i^0 = 0$ . One thus have a linearized version of Eq.2.1.7, which is known as the Debye-Hückel equation:

$$\nabla^2 \Psi(\vec{r}) = \left[ \sum_i \frac{z_i^2 e^2 c_i^0}{\epsilon_0 \epsilon_r k_B T} \right] \Psi(\vec{r}) . \quad (2.1.11)$$

From this approximation, one can identify that the term between brackets is the inverse of a distance squared. We can thus define a distance  $\ell_D$ , the Debye length such as:

$$\ell_D = \sqrt{\sum_i \frac{\epsilon_0 \epsilon_r k_B T}{z_i^2 e^2 c_i^0}} . \quad (2.1.12)$$

The Debye length is the characteristic length of the double-layer, and, the electrostatic interactions. For a monovalent electrolyte, at 25 °C (298 K), the Debye length of aqueous solution is:

$$\begin{aligned} \ell_D &= \sqrt{\frac{\epsilon_0 \epsilon_r k_B T}{2c_s^0 e^2}} = \sqrt{\frac{8.854 \times 10^{-12} \times 78.4 \times 1.381 \times 10^{-23} \times 298}{2 \times (1.602 \times 10^{-19})^2 \times 6.022 \times 10^{26} M}} \\ &= 0.304 \times 10^{-9} / \sqrt{M} \text{ m ,} \end{aligned} \quad (2.1.13)$$

with M the molar concentration ( $1 \text{ M} = 1 \text{ mol.L}^{-1}$  corresponding to a number density of  $c_s^0 = 6.022 \times 10^{26} \text{ m}^{-3}$ ). Thus, for a salty concentration we have  $\ell_D = 0.304 / \sqrt{[\text{NaCl}]} \text{ nm}$ . For example, for NaCl solution, one can have  $\ell_D = 100 \text{ nm}$  for a concentration  $[\text{NaCl}] = 9.2 \mu\text{M}$  and  $\ell_D = 10 \text{ nm}$  for a concentration  $[\text{NaCl}] = 9.2 \text{ mM}$ .

Finally, the Debye-Hückel approximation finally writes:

$$\nabla^2 \Psi(\vec{r}) = \kappa^2 \Psi(\vec{r}) , \quad (2.1.14)$$

with  $\kappa = 1/\ell_D$ . Using the latter approximation one can compute the electrostatic potential around a sphere. Let us consider a perfect sphere of radius  $a$  and charge  $Qe$  of charge density  $\sigma = Qe/4\pi a^2$ . With  $Q$  being the number of charge on the surface. Since the system has a spherical symmetry, one has  $\Psi(\vec{r}) = \Psi(r)$  with  $r = |\vec{r}|$ . Using the Laplacian operator  $\nabla^2$  in the spherical coordinates, Eq.2.1.14 writes:

$$\frac{1}{r^2} \left[ \frac{\partial}{\partial r} \left( r^2 \frac{\partial \Psi(r)}{\partial r} \right) \right] = \kappa^2 \Psi(r) , \quad (2.1.15)$$

which has a general solution:

$$\Psi(r) = C_1 \frac{\exp(\kappa r)}{r} + C_2 \frac{-\exp(\kappa r)}{r} \quad (2.1.16)$$

For one sphere, the electrostatic field vanishes at infinity such as  $C_1 = 0$ , such it has the form of a Yukawa potential:

$$\Psi(r) = C_2 \frac{-\exp(\kappa r)}{r} . \quad (2.1.17)$$

Additionally, at the surface of a charged sphere, the electrostatic potential satisfies:

$$\left. \frac{\partial \Psi(r)}{\partial r} \right|_{r=a} = \frac{Qe}{4\pi\epsilon_0\epsilon_r a^2} = \frac{\sigma}{\epsilon_0\epsilon_r} . \quad (2.1.18)$$

By applying the latter boundary condition to Eq.2.1.17 we find:

$$\Psi(r) = \frac{\sigma a^2}{\epsilon_0\epsilon_r} \frac{\exp(\kappa a)}{1 + \kappa a} \frac{\exp(-\kappa r)}{r} \quad (2.1.19)$$

This solution can be used to determine the electrostatic field between two spheres. Indeed, if we suppose that the presence of a second sphere, do not interfere with the distribution of ions in the double layer of the other. We can thus use the superposition approximation to write the potential  $\Psi_2(z)$  between two spheres surfaces. Where  $z$  is the distance between the 2 colloids. For two spheres of charge  $\sigma_1$  and  $\sigma_2$  and radius  $a_1$  and  $a_2$ ,  $\Psi_2(z)$  writes [69]:

$$\Psi(z) = \frac{4\pi}{\epsilon_0\epsilon_r} \left( \frac{\sigma_1 a_1^2}{1 + \kappa a_1} \right) \left( \frac{\sigma_2 a_2^2}{1 + \kappa a_2} \right) \frac{\exp(-\kappa z)}{a_1 + a_2 + z} . \quad (2.1.20)$$

From the latter equation, it is possible to write the electrostatic field between a wall and a spherical colloid, by setting one of the radius to infinity. Doing so and multiplying by  $e$ , one can have the electrostatic potential  $E_{elec}(z)$  between a Brownian particle and the wall:

$$E_{elec}(z) = B e^{-\frac{z}{\ell_D}} . \quad (2.1.21)$$

Where  $B$  is the constant that represent the surface charges, for sphere of radius  $a$  and charge  $\sigma_1$  and a wall of charge  $\sigma_2$ , one has:

$$B = \frac{4\pi}{\epsilon_0\epsilon_r} \left( \frac{\sigma_1 a^2}{1 + \kappa a} \right) \frac{\sigma_2}{\kappa} . \quad (2.1.22)$$

Additionally,  $B$  is often written as a function of the surfaces potential as [CITE PRIEVES]:

$$B = 16\epsilon_r\epsilon_0 \left( \frac{k_B T}{e} \right) \tanh \left( \frac{e\phi_1}{4k_B T} \right) \tanh \left( \frac{e\phi_2}{4k_B T} \right), \quad (2.1.23)$$

where  $\phi_1$  and  $\phi_2$  are the Stern potentials of the sphere and the wall surfaces. Typical values for  $B$  ranges from  $1 k_B T$  to  $50 k_B T$ . In our study we will keep  $B$  to describe the electrostatic energy potential as it complicated to decouple the  $\sigma_1$  and  $\sigma_2$  when the colloid and wall's surface materials are different [70]. However, this is not impossible and is the idea of future work.

### Van der Waals interactions

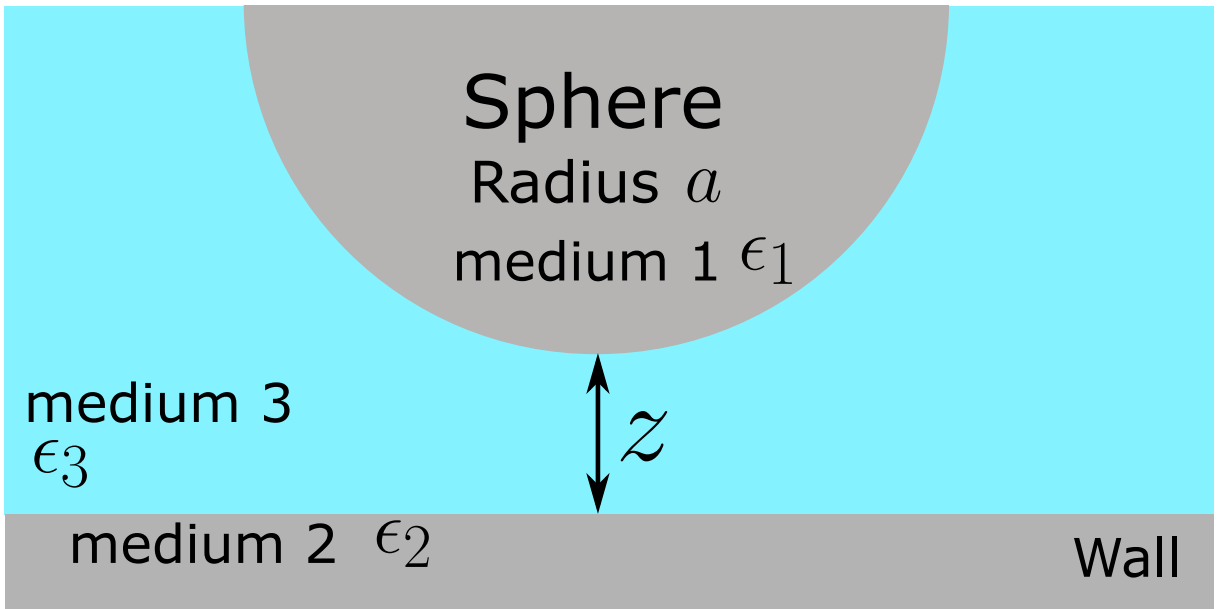


Figure 8: A colloid of radius  $a$  separated from a wall from a distance  $z$ . The colloid material has a static dielectric constant  $\epsilon_1$ , the wall  $\epsilon_2$  and the solution  $\epsilon_3$ .

In the DLVO theory, the Van der Waals forces describes the interaction between colloids at very short range. This forces are mainly attractive and in our case having Van der Waals interactions would lead to the particles stick to the wall. The Van der Waals potential energy  $E_{VdW}$  for a spherical colloid of radius  $a$ , at a height  $z$  at a few nanometers ( $< 5$  nm) to the surface [68]:

$$E_{VdW} = -\frac{Aa}{6z} \quad (2.1.24)$$

where  $A$  is the retarded Hamaker constant. For our system, where the particle, medium and wall are different medium as schematized in Fig.8. In that case the Hamaker constant

writes [68]:

$$A = \frac{3}{4}k_B T \left( \frac{\epsilon_1 - \epsilon_3}{\epsilon_1 + \epsilon_3} \right) \left( \frac{\epsilon_2 - \epsilon_3}{\epsilon_2 + \epsilon_3} \right) + \frac{3h}{4\pi} \int_{\nu_1}^{\infty} \left( \frac{\epsilon_1(i\nu) - \epsilon_3(i\nu)}{\epsilon_1(i\nu) + \epsilon_3(i\nu)} \right) \left( \frac{\epsilon_2(i\nu) - \epsilon_3(i\nu)}{\epsilon_2(i\nu) + \epsilon_3(i\nu)} \right) d\nu , \quad (2.1.25)$$

where  $\epsilon_1$ ,  $\epsilon_2$  and  $\epsilon_3$  are the static dielectric constants of the three media,  $\epsilon(i\nu)$  are the imaginary dielectric constant at a frequency  $\nu$  and  $\nu_n = (2\pi k_B T n / h) = 4 \times 10^{13} \text{ ns}^{-1}$  at 300 K; and;  $h$  is the Plank's constant. The first term fives the zero-frequency energy of the van der Waals interaction and the second term the dispersion energy. However, since the static dielectric of water is large compared to the other terms [68], one can approximate the Hamaker constant of our system to only the zero-frequency term:

$$A = \frac{3}{4} 1.381 \times 10^{-23} \times 298 \left( \frac{2.5 - 80}{2.5 + 80} \right) \left( \frac{5 - 80}{5 + 80} \right) \simeq 2.48 \times 10^{-21} \text{ J} = 0.62 k_B T . \quad (2.1.26)$$

Since  $A$  is positive we correctly have an attractive Van der Waals force, this case will always be the case due to the high dielectric constant of water. More over, the zero-frequency Van der Waals force is mainly due to electrostatic interaction and is thus screened by electrolytes, we thus need to add a factor  $\approx e^{-z/\ell_D}$  to the Van der Waals forces. Also, it has been proposed [71] that to compute the force at higher distances, one should add a second factor, to account for the retarded Van der Waals force of  $\simeq (1 + 11z/100\text{nm})^{-1}$ .

All the effects added together we can see that the Van der Waals forces will play a role only a few nanometer ( $< 10$  nm) as it is commonly observed [M,P]. In our experiments, the Debye length  $\ell_D$  ( $> 20$  nm) is large enough for the particle to avoid this region, in the following of this work the Van der Waals interactions will be neglected. To study the Van der Waals interactions with Brownian motion, it is possible, if one add enough salt to have  $\ell_D \simeq 1$  nm. However, with such a short Debye length, all the colloids would stick to the surface and between each other. However, we have experimentally observed some dynamics on the sucked particles, further work on this movement could lead to interesting determination of the near-wall potential.

## Total potential and equilibrium distribution

If we combine the gravitational and electrostatic interactions the particules lies into a total energy potential  $U(z)$ :

$$U(z) = U_g + U_{\text{elec}} \quad (2.1.27)$$

By combining Eqs.2.1.3, 2.1.21 and 2.1.27, and also adding the condition that the particle can't go inside the wall  $U(z)$  finally writes:

$$\frac{U(z)}{k_B T} = \begin{cases} B e^{-\frac{z}{\ell_D}} + \frac{z}{\ell_B}, & \text{for } z > 0 \\ +\infty, & \text{for } z \leq 0 \end{cases}, \quad (2.1.28)$$

From this total potential energy, one can then construct the Gibbs-Boltzmann distribution to write the equilibrium PDF of position  $P_{\text{eq}}(z)$ :

$$P_{\text{eq}}(z) = A \exp\left(-\frac{U(z)}{k_B T}\right), \quad (2.1.29)$$

where  $A$  is a normalization constant such that  $\int_0^\infty P_{\text{eq}}(z) dz = 1$ . Given an array of heights  $z_i$  one can use compute  $P_{\text{eq}}$  using the following Python snippet, where the  $A$  is computed using the `np.trapz` function. An example of a theoretical energy potential and PDF of position can be seen Fig.9 for  $\ell_B = 500$  nm,  $B = 4 k_B T$  and  $\ell_D = 50$  nm.

---

```

1 import numpy as np
2
3 def _Peq(z):
4     if z <= 0:
5         return 0
6     else:
7         return np.exp(-(B * np.exp(-z / 1d) + z / 1b))
8
9
10 def Peq(z):
11     P = np.array([_Peq(zi) for zi in z])
12     return P / np.trapz(P,z)

```

---

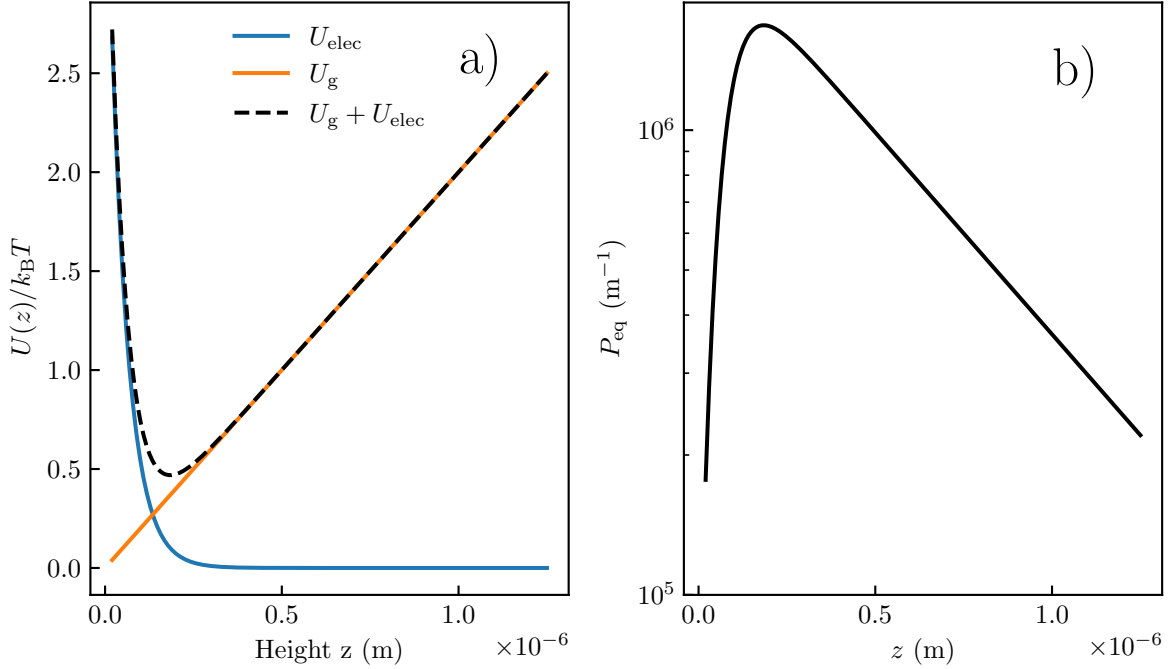


Figure 9: a) Potential energy of a colloid of Boltzmann length  $\ell_B = 500$  nm. The electrostatic potential  $U_{\text{elec}}$  is here characterized by a surface charge constant  $B = 4 k_B T$  and a Debye length  $\ell_D = 50$  nm. b) Corresponding Gibbs-Boltzmann equilibrium distribution of position.

### 2.1.3 Local diffusion coefficient

As we have seen in the Chapter 2, for a freely diffusing colloid in bulk the diffusion coefficient is given by Eq.1.2.12 and is a constant. However, when a particle is confined, the diffusion is hindered, this means that the diffusion coefficient vary with the height of the particle and becomes anisotropic. One of the first measurement that has been done by Faucheux and Libchaber [13]. As we can see on the Fig.10, using a microscope, they tracked Brownian colloids in two dimensions, and, measured the average coefficient diffusion for different confinement constant  $\gamma = (\langle z \rangle_t - a)/a$ . Finally, on the Fig.10, one can observe that the diffusion coefficient parallel to the surface decreases as the particle get closer to the wall, and, seems to saturate around  $0.3D_0$  for high confinement.

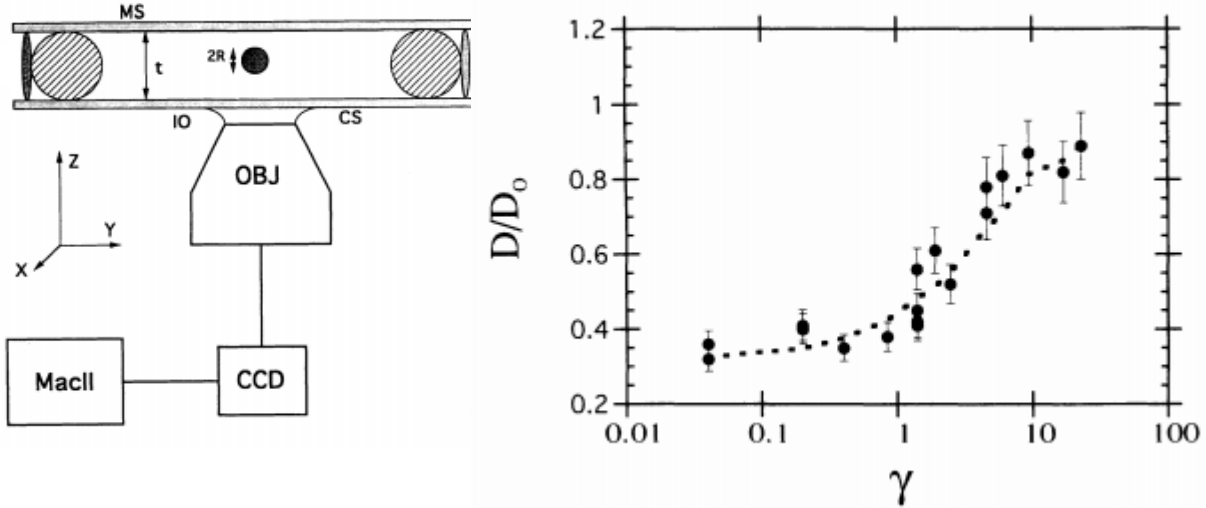


Figure 10: Figure extracted from [13], on the left is the experimental setup used. It is an inverted microscope used in order to track particle of size  $2R$  inside a cell of thickness  $t$ . On the right is their final result, where they measure the diffusion parallel coefficient  $D_{\perp}$  given by Eq.2.1.41, here normalized by  $D_0$  the bulk diffusion coefficient as a function of  $\gamma$  a confinement constant  $\gamma = (\langle z \rangle - a)/a$ .

To understand the reason of this hindered diffusion coefficient, let us start by writing the diffusion coefficient  $D$  using the fluctuation dissipation theorem:

$$D = \mu k_B T , \quad (2.1.30)$$

with:

$$\mu = \frac{v_{\text{sphere}}}{F_{\text{drag}}} , \quad (2.1.31)$$

where  $v_{\text{sphere}}$  is the terminal velocity to an applied force  $F_{\text{drag}}$ . For a spherical colloid of radius  $R$  moving at a velocity  $v_{\text{sphere}}$  the drag force in bulk  $F_{\text{drag}}^{\text{B}}$  is given by the Stockes' law:

$$F_{\text{drag}}^{\text{B}} = c\pi\eta av_{\text{sphere}} , \quad (2.1.32)$$

where  $c$  is a constant that depends on the boundary conditions imposed at the surface of

the colloid, typically  $c = 6$  for no-slip and  $c = 4$  (such as air bubbles for example) for slip boundary conditions. Combining Eqs.2.1.30, 2.1.31 and 2.1.32 for a freely diffusing hard sphere in bulk we retrieve Eq.1.2.12:

$$D_0 = \frac{k_B T}{6\pi\eta a} . \quad (2.1.33)$$

The Stocke's drag force can be computed by solving the Navier-Stokes equation:

$$\rho \left[ \frac{\partial \vec{v}}{\partial} + (\vec{v} \cdot \nabla \vec{v}) \right] + \nabla p = \eta \nabla^2 \vec{v} , \quad (2.1.34)$$

and the continuity equation for incrompressible fluids:

$$\nabla \cdot \vec{v} = 0 \quad (2.1.35)$$

where  $\vec{v}$  and  $p$  is the velocity and pressure fields  $\rho$  is the density of the fluid. When the Reynolds number  $Re = \rho a v_{\text{sphere}} / \eta \ll 1$ , the first two terms are inertial and are negligibly small compared to the viscous term  $\eta \nabla^2 \vec{v}$ . In that case, the Navier-Stokes Eq.2.1.34, is simplified to the Stockes flow formula:

$$\nabla p = \eta \nabla^2 \vec{v} \quad (2.1.36)$$

The diffusion coefficient for a freely diffusing spherical colloid in bulk can thus be found by solving Eqs.2.1.36 and 2.1.35 by having a no-slip boundary condition on the particle surface and the velocity vanishing at infinity. However, in the case of a confined particle, there is an additional no-slip condition at the wall surface. Indeed, as shown on the Fig.11, the fluid velocity drop to zero at the wall surface, with a shear rate:

$$\dot{\gamma} = \frac{\partial v_{\text{sphere}}}{\partial z} \quad (2.1.37)$$

This shear rate, due to the presence of the wall introduce a shear force  $F(z) = \simeq \eta \dot{\gamma}(z)$  acting on the particle. Hence, the drag force acting on the particle will increase inversely with the distance to the wall, due to additional hydrodynamic pressure arising from velocity gradients. At the macro scale, this effect can be seen with a frisbee, indeed, as it

gets closer to the grounds, hydrodynamic pressure increases due to air velocity gradient and one can observe that the frisbee seems to stop falling and continue to glide really near the ground's surface.

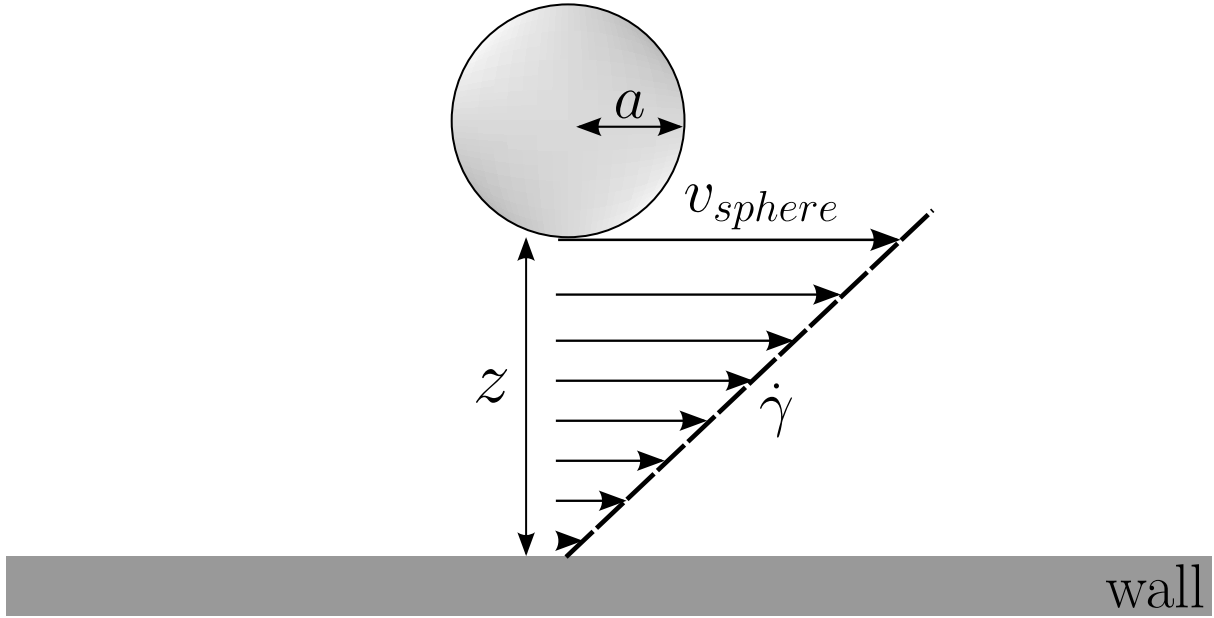


Figure 11: Schematic representation of a spherical colloid moving near a wall and the induced shear rate  $\dot{\gamma}$ .

A colloid diffusing near a wall thus experience a local drag force that depends on both it's distance to the wall  $z$  and the movement direction. Thanks to the linearity of the Stokes equation, one can separate this local drag force for motion parrallel and perpendicular to the wall. As the presence of the wall correct the drag force from a multiplicative coefficient, the confinement effect often expressed as an effective viscosity:

$$\eta_{\perp}(z) = \eta\lambda_{\perp}(z) , \text{ and, } \eta_{\parallel}(z) = \eta\lambda_{\parallel}(z) , \quad (2.1.38)$$

where  $\lambda_{\perp}$  and  $\lambda_{\parallel}$  are respectively perpendicular and parallel correction factor to the drag force due to the presence of the wall. Due to this correction, the diffusion coefficients for parallel and perpendicular motion relative to the wall writes:

$$D_{\perp}(z) = \frac{D_0}{\lambda_{\perp}(z)} , \text{ and, } D_{\parallel}(z) = \frac{D_0}{\lambda_{\parallel}(z)} . \quad (2.1.39)$$

For a no-slip boundary conditions imposed at the wall and the surface of the colloid, Brenner [72] obtained for perpendicular motion:

$$\lambda_{\perp}(z) = \frac{4}{3} \sinh \beta \sum_{n=1}^{\infty} \frac{n(n+1)}{(2n-1)(2n+3)} \left[ \frac{2 \sinh(2n+1)\beta + (2n+1)\sinh 2\beta}{4 \sinh^2(n+1/2)\beta - (2n+1)^2 \sinh^2 \beta} - 1 \right], \quad (2.1.40)$$

where  $\beta = \cosh^{-1}((z+a)/a)$ . The solution for the diffusion parallel to the wall, Faxén found [73]:

$$\lambda_{\parallel}(z) = \left[ 1 - \frac{9}{16}\xi + \frac{1}{8}\xi^3 - \frac{45}{256}\xi^4 - \frac{1}{16}\xi^5 \right]^{-1}, \quad (2.1.41)$$

where  $\xi = a/(z+a)$ . Eqs.2.1.40 and 2.1.41 are precise for all  $z$ . However, the solution for the perpendicular motion can be quite complex to compute as it is an infinite series, to be computed numerically it requires a software that enable arbitrary-precision floating-point arithmetic<sup>4</sup> — such as Mathematica or the `mpmath` Python's module for example.  $D_{\perp}$  can be evaluated using the following Python snippet, where `nsum` function is used to compute the infinite sum:

---

```

1 from mpmath import nsum
2
3 def Dz(eta, z, a):
4     a = (z + a) / a
5     beta = float(acosh(a))
6     summ = nsum(
7         lambda n: (n * (n + 1) / ((2 * n - 1) * (2 * n + 3)))
8         *
9         (
10            (2 * sinh((2 * n + 1) * xi) + (2 * n + 1) * sinh(2 * beta))
11            /
12            (4 * (sinh((n + 1 / 2) * beta) ** 2)
13             - ((2 * n + 1) ** 2) * (sinh(beta) ** 2)
14            )
15        )
16        -
17    ),
18    [0, inf],
19    )
20     summ = float(summ)
21 return kT / (6 * pi * eta * 4 / 3 * float(sinh(beta)) * summ * a)

```

---

<sup>4</sup> Arbitrary-precision floating-point arithmetic enables to evaluate mathematical expression with any precision, in other words, any number of digits.

To simplify the computation of  $\lambda_{\perp}$ , Goldman *et al.* [74] showed that Eq.2.1.40 can be Padé approximated, giving:

$$\lambda_{\perp} = \frac{6z^2 + 9az + 2a^2}{6z^2 + 2az} . \quad (2.1.42)$$

In the near-wall regime, such that  $z \ll a$ , it is also possible to further approximate  $\lambda_{\perp}$  to:

$$\lambda_{\perp} = \frac{a}{z} . \quad (2.1.43)$$

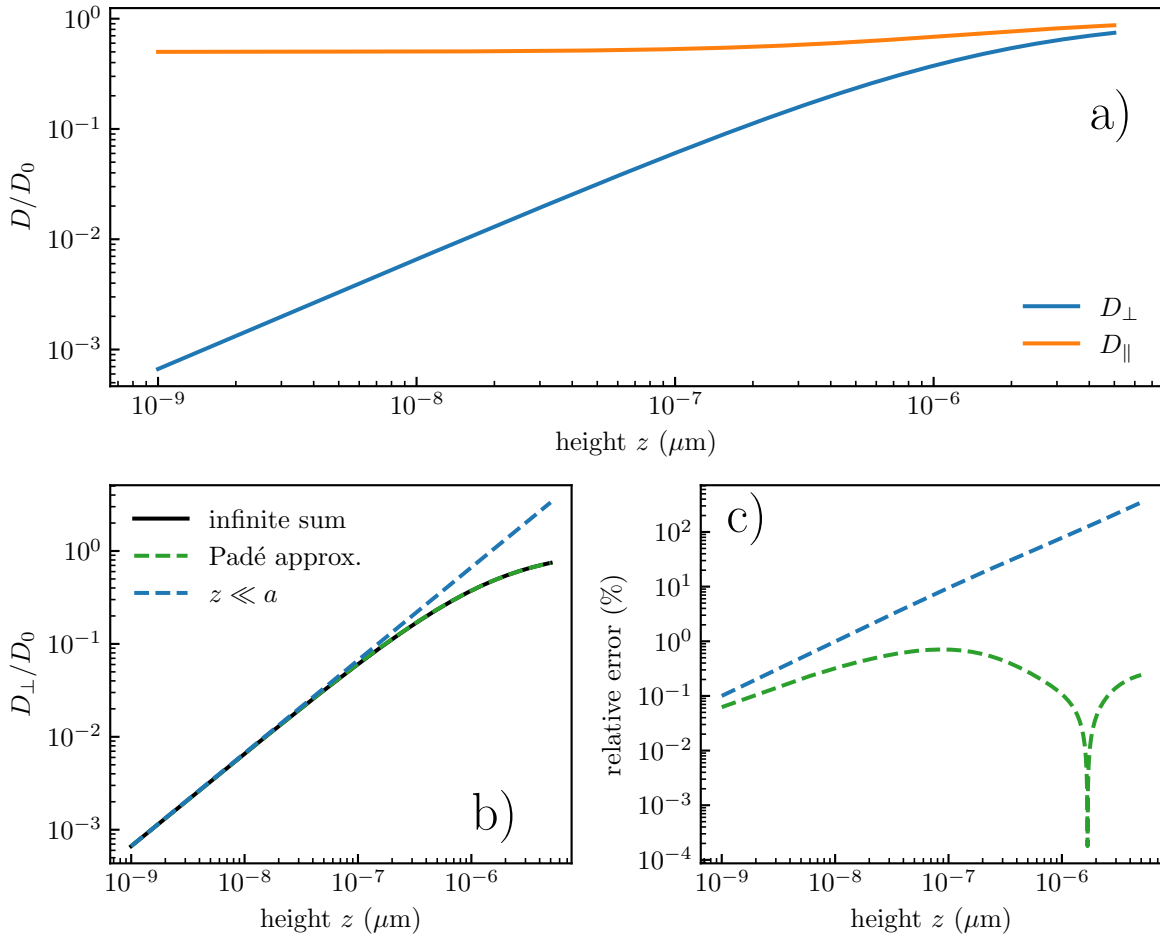


Figure 12: a) Parallel and perpendicular hindered relative diffusion coefficient for a colloidal particle of radius  $a = 1.5 \mu\text{m}$ . b) Perpendicular hindered relative diffusion coefficient for a colloid particle of radius  $a = 1.5 \mu\text{m}$ . In black the exact solution given by the infinite sum Eq.2.1.40. In green the Padé approximation, Eq.2.1.42 and in blue the near wall regime Eq.2.1.43. c) Relative error of the perpendicular hindered coefficient.

The Padé approximation and the near-wall approximation for the hindered diffusion are

plotted on Fig.12-b). The Padé approximation fits really well with the exact solution given by the infinite sum Eq.2.1.40, the near-wall approximation fits well when  $z < a/10$ . To check how precise the approximation are, it is possible to plot the relative error as in the Fig.12-c). The Padé approximation shows a precision up to 1%, thus, in the following of this work, when we refer to any evaluation of the hindered perpendicular diffusion, the Padé approximation will be used.

#### 2.1.4 Langevin equation for the confined Brownian motion

Now that the external forces acting on the particle and hindered diffusion coefficient is known, we rewrite the overdamped Langevin Eq.1.3.10 equation as:

$$V_t^i dt = -\frac{1}{\gamma(z)} \frac{\partial U(z)}{\partial x_i} dt + \sqrt{2D_i(z)} dB_t . \quad (2.1.44)$$

where  $\gamma(z) = 6\pi\eta_i(z)a$  and  $i$  denotes three spatial directions,  $x$ ,  $y$  and  $z$ <sup>5</sup>, and,  $dB_t$  still is a Gaussian distribution satisfying  $\langle dB_t \rangle = 0$  and  $\langle dB_t^2 \rangle = dt$ . As we have discussed previously, the potential  $U$  only varies along the  $z$  axis, thus, the external forces only acts on the particle on the  $z$  axis while the particle diffuses freely along the  $x$  and  $y$  axis.

#### 2.1.5 Spurious drift

It is interesting to observe that due to the hindered diffusion the magnitude of the Langevin force,  $\sqrt{2D_i(z)}$ , is not anymore a constant, but varies with the height of the particle. This effect is called multiplicative noise and will have some interesting effects on the dynamics properties of the Brownian motion. To show the effects of the multiplicative noise, one can integrate over a time  $\tau$  the Eq.2.1.44, in the absence of the external force one has:

$$\Delta x_i = \int_{t_0}^{t_0+\tau} \sqrt{2D_i(z)} dB_t \quad (2.1.45)$$

where  $\Delta x_i$  is a space increment. However, the noise term is not well-defined and the time at which the magnitude of the force  $\sqrt{2D_i(z)}$  in the integration Eq.2.1.45 needs to be

---

<sup>5</sup> Where the previously determined  $\eta_{||}$  and  $D_{||}$  correspond to the  $x$  and  $y$  axis and  $\eta_{\perp}$  and  $D_{\perp}$  correspond to the  $z$  axis.

specified.

### 2.1.6 Numerical simulation of confined Brownian motion

## 2.2 Experimental study

### 2.2.1 MSD

### 2.2.2 Non-gaussian dynamics - Displacement distribution

### 2.2.3 Local diffusion coefficient inference

### 2.2.4 Precise potential inference using multi-fitting technique

### 2.2.5 Measuring external forces using the local drifts

## 2.3 conclusion

## References

- [1] R. Baraniuk, D. Donoho, and M. Gavish, “The science of deep learning”, Proceedings of the National Academy of Sciences **117**, Publisher: National Academy of Sciences Section: Introduction, 30029–30032 (2020).
- [2] B. Lemieux, A. Aharoni, and M. Schena, “Overview of DNA chip technology”, Molecular Breeding **4**, 277–289 (1998).
- [3] Á. Ríos, M. Zougagh, and M. Avila, “Miniaturization through lab-on-a-chip: utopia or reality for routine laboratories? a review”, Analytica Chimica Acta **740**, 1–11 (2012).
- [4] A. Einstein, “Über die von der molekularkinetischen Theorie der Wärme geforderte Bewegung von in ruhenden Flüssigkeiten suspendierten Teilchen”, Annalen der Physik **vol. 4, t. 17** (1905).
- [5] J. Perrin, *Les Atomes*, Google-Books-ID: A0ltBQAAQBAJ (CNRS Editions, Nov. 14, 2014), 199 pp.
- [6] B. U. Felderhof, “Effect of the wall on the velocity autocorrelation function and long-time tail of brownian motion †”, The Journal of Physical Chemistry B **109**, 21406–21412 (2005).
- [7] M. V. Chubynsky and G. W. Slater, “Diffusing diffusivity: a model for anomalous, yet brownian, diffusion”, Physical Review Letters **113**, 098302 (2014).
- [8] A. V. Chechkin, F. Seno, R. Metzler, and I. M. Sokolov, “Brownian yet non-gaussian diffusion: from superstatistics to subordination of diffusing diffusivities”, Physical Review X **7**, 021002 (2017).
- [9] C. I. Bouzigues, P. Tabeling, and L. Bocquet, “Nanofluidics in the debye layer at hydrophilic and hydrophobic surfaces”, Physical Review Letters **101**, Publisher: American Physical Society, 114503 (2008).
- [10] L. Joly, C. Ybert, and L. Bocquet, “Probing the nanohydrodynamics at liquid-solid interfaces using thermal motion”, Physical Review Letters **96**, Publisher: American Physical Society, 046101 (2006).
- [11] J. Mo, A. Simha, and M. G. Raizen, “Brownian motion as a new probe of wettability”, The Journal of Chemical Physics **146**, Publisher: American Institute of Physics, 134707 (2017).

- [12] E. R. Dufresne, T. M. Squires, M. P. Brenner, and D. G. Grier, “Hydrodynamic coupling of two brownian spheres to a planar surface”, *Physical Review Letters* **85**, Publisher: American Physical Society, 3317–3320 (2000).
- [13] L. P. Faucheux and A. J. Libchaber, “Confined brownian motion”, *Physical Review E* **49**, 5158–5163 (1994).
- [14] E. R. Dufresne, D. Altman, and D. G. Grier, “Brownian dynamics of a sphere between parallel walls”, *EPL (Europhysics Letters)* **53**, Publisher: IOP Publishing, 264 (2001).
- [15] H. B. Eral, J. M. Oh, D. v. d. Ende, F. Mugele, and M. H. G. Duits, “Anisotropic and hindered diffusion of colloidal particles in a closed cylinder”, *Langmuir* **26**, Publisher: American Chemical Society, 16722–16729 (2010).
- [16] P. Sharma, S. Ghosh, and S. Bhattacharya, “A high-precision study of hindered diffusion near a wall”, *Applied Physics Letters* **97**, Publisher: American Institute of Physics, 104101 (2010).
- [17] J. Mo, A. Simha, and M. G. Raizen, “Broadband boundary effects on brownian motion”, *Physical Review E* **92**, 062106 (2015).
- [18] M. Matse, M. V. Chubynsky, and J. Bechhoefer, “Test of the diffusing-diffusivity mechanism using near-wall colloidal dynamics”, *Physical Review E* **96**, 042604 (2017).
- [19] D. C. Prieve, “Measurement of colloidal forces with TIRM”, *Advances in Colloid and Interface Science* **82**, 93–125 (1999).
- [20] A. Banerjee and K. Kihm, “Experimental verification of near-wall hindered diffusion for the brownian motion of nanoparticles using evanescent wave microscopy”, *Physical review. E, Statistical, nonlinear, and soft matter physics* **72**, 042101 (2005).
- [21] S. Sainis, V. Germain, and E. Dufresne, “Statistics of particle trajectories at short time intervals reveal fN-scale colloidal forces”, *Physical review letters* **99**, 018303 (2007).
- [22] G. Volpe, L. Helden, T. Brettschneider, J. Wehr, and C. Bechinger, “Influence of noise on force measurements”, *Physical Review Letters* **104**, 170602 (2010).
- [23] M. Li, O. Sentissi, S. Azzini, G. Schnoering, A. Canaguier-Durand, and C. Genet, “Subfemtonewton force fields measured with ergodic brownian ensembles”, *Physical Review A* **100**, 063816 (2019).

- [24] S. K. Sainis, V. Germain, and E. R. Dufresne, “Statistics of particle trajectories at short time intervals reveal fN-scale colloidal forces”, *Physical Review Letters* **99**, 018303 (2007).
- [25] B. Robert, “XXVII. a brief account of microscopical observations made in the months of june, july and august 1827, on the particles contained in the pollen of plants; and on the general existence of active molecules in organic and inorganic bodies”, *The Philosophical Magazine* **4**, Taylor & Francis, 161–173 (1828).
- [26] S. Peter, “Brownian motion”, **Brownian motion**.
- [27] J. Perrin, “Mouvement brownien et molécules”, *J. Phys. Theor. Appl.* **9**, 5–39 (1910).
- [28] A. Genthon, “The concept of velocity in the history of brownian motion”, *The European Physical Journal H* **45**, 49–105 (2020).
- [29] P. Langevin, “Sur la théorie du mouvement brownien”, *C. R. Acad. Sci. (Paris)* **146**, 530–533 **65**, 1079–1081 (1908).
- [30] R. Durrett, *Probability: theory and examples*, 5th ed., Cambridge Series in Statistical and Probabilistic Mathematics (Cambridge University Press, Cambridge, 2019).
- [31] D. Freedman and P. Diaconis, “On the histogram as a density estimator:l 2 theory”, *Zeitschrift für Wahrscheinlichkeitstheorie und Verwandte Gebiete* **57**, 453–476 (1981).
- [32] C. Fabry and A. Pérot, “Théorie et application d'une nouvelle méthode de spectroscopie interferentielle.”, *Ann. Chim. Phys.*, **7** (1899).
- [33] A. Perot and C. Fabry, “On the application of interference phenomena to the solution of various problems of spectroscopy and metrology”, *The Astrophysical Journal* **9**, 87 (1899).
- [34] A. A. Michelson and E. W. Morley, “On the relative motion of the earth and the luminiferous ether”, *American Journal of Science* **s3-34**, Publisher: American Journal of Science Section: Extraterrestrial geology, 333–345 (1887).
- [35] LIGO Scientific Collaboration and Virgo Collaboration et al., “GW151226: observation of gravitational waves from a 22-solar-mass binary black hole coalescence”, *Physical Review Letters* **116**, in collab. with B. P. Abbott, Publisher: American Physical Society, 241103 (2016).

- [36] A. S. Curtis, “THE MECHANISM OF ADHESION OF CELLS TO GLASS. a STUDY BY INTERFERENCE REFLECTION MICROSCOPY”, *The Journal of Cell Biology* **20**, 199–215 (1964).
- [37] T. J. Filler and E. T. Peuker, “Reflection contrast microscopy (RCM): a forgotten technique?”, *The Journal of Pathology* **190**, 635–638 (2000).
- [38] P. A. Siver and J. Hinsch, “THE USE OF INTERFERENCE REFLECTION CONTRAST IN THE EXAMINATION OF DIATOM VALVES”, *Journal of Phycology* **36**, 616–620 (2000).
- [39] I. Weber, “[2] reflection interference contrast microscopy”, in *Methods in enzymology*, Vol. 361, Biophotonics, Part B (Academic Press, Jan. 1, 2003), pp. 34–47.
- [40] L. Limozin and K. Sengupta, “Quantitative reflection interference contrast microscopy (RICM) in soft matter and cell adhesion”, *Chemphyschem: A European Journal of Chemical Physics and Physical Chemistry* **10**, 2752–2768 (2009).
- [41] F. Nadal, A. Dazzi, F. Argoul, and B. Pouliquen, “Probing the confined dynamics of a spherical colloid close to a surface by combined optical trapping and reflection interference contrast microscopy”, *Applied Physics Letters* **79**, 3887–3889 (2002).
- [42] J. Raedler and E. Sackmann, “On the measurement of weak repulsive and frictional colloidal forces by reflection interference contrast microscopy”, *Langmuir* **8**, 848–853 (1992).
- [43] H. S. Davies, D. Débarre, N. El Amri, C. Verdier, R. P. Richter, and L. Bureau, “Elastohydrodynamic lift at a soft wall”, *Physical Review Letters* **120**, 198001 (2018).
- [44] C. F. Bohren and D. R. Huffman, *Absorption and scattering of light by small particles* (Wiley, Apr. 1998).
- [45] H. J. W. Strutt, “LVIII. on the scattering of light by small particles”, *The London, Edinburgh, and Dublin Philosophical Magazine and Journal of Science* **41**, Publisher: Taylor & Francis \_eprint: <https://doi.org/10.1080/14786447108640507>, 447–454 (1871).
- [46] L. Lorenz, *Lysbevægelsen i og uden for en af plane Lysbølger belyst Kugle*, Google-Books-ID: hnE7QwAACAAJ (1890), 62 pp.
- [47] G. Mie, “Beiträge zur optik trüber medien, speziell kolloidaler metallösungen”, *Annalen der Physik* **330**, \_eprint: <https://onlinelibrary.wiley.com/doi/pdf/10.1002/andp.19083300302> 377–445 (1908).

- [48] B. Ovryn and S. H. Izen, “Imaging of transparent spheres through a planar interface using a high-numerical-aperture optical microscope”, *Journal of the Optical Society of America A* **17**, 1202 (2000).
- [49] S.-H. Lee, Y. Roichman, G.-R. Yi, S.-H. Kim, S.-M. Yang, A. v. Blaaderen, P. v. Oostrum, and D. G. Grier, “Characterizing and tracking single colloidal particles with video holographic microscopy”, *Optics Express* **15**, Publisher: Optical Society of America, 18275–18282 (2007).
- [50] J. Katz and J. Sheng, “Applications of holography in fluid mechanics and particle dynamics”, *Annual Review of Fluid Mechanics* **42**, \_eprint: <https://doi.org/10.1146/annurev-fluid-121108-145508>, 531–555 (2010).
- [51] P. Gregory, *Bayesian logical data analysis for the physical sciences: a comparative approach with mathematica® support*, Google-Books-ID: idkLAQAAQBAJ (Cambridge University Press, Apr. 14, 2005), 496 pp.
- [52] T. G. Dimiduk and V. N. Manoharan, “Bayesian approach to analyzing holograms of colloidal particles”, *Optics Express* **24**, Publisher: Optical Society of America, 24045–24060 (2016).
- [53] W. J. Lentz, “Generating bessel functions in mie scattering calculations using continued fractions”, *Applied Optics* **15**, Publisher: Optical Society of America, 668–671 (1976).
- [54] J. Fung and V. N. Manoharan, “Holographic measurements of anisotropic three-dimensional diffusion of colloidal clusters”, *Physical Review E* **88**, 020302 (2013).
- [55] A. Wang, T. G. Dimiduk, J. Fung, S. Razavi, I. Kretzschmar, K. Chaudhary, and V. N. Manoharan, “Using the discrete dipole approximation and holographic microscopy to measure rotational dynamics of non-spherical colloidal particles”, *Journal of Quantitative Spectroscopy and Radiative Transfer* **146**, 499–509 (2014).
- [56] R. W. Perry, G. Meng, T. G. Dimiduk, J. Fung, and V. N. Manoharan, “Real-space studies of the structure and dynamics of self-assembled colloidal clusters”, *Faraday Discussions* **159**, Publisher: The Royal Society of Chemistry, 211–234 (2013).
- [57] T. G. Dimiduk, R. W. Perry, J. Fung, and V. N. Manoharan, “Random-subset fitting of digital holograms for fast three-dimensional particle tracking”, *Applied Optics* **53**, G177 (2014).

- [58] A. Yevick, M. Hannel, and D. G. Grier, “Machine-learning approach to holographic particle characterization”, *Optics Express* **22**, 26884 (2014).
- [59] M. D. Hannel, A. Abdulali, M. O’Brien, and D. G. Grier, “Machine-learning techniques for fast and accurate feature localization in holograms of colloidal particles”, *Optics Express* **26**, Publisher: Optical Society of America, 15221–15231 (2018).
- [60] L. E. Altman and D. G. Grier, “CATCH: characterizing and tracking colloids holographically using deep neural networks”, *The Journal of Physical Chemistry B* **124**, Publisher: American Chemical Society, 1602–1610 (2020).
- [61] L. Wilson and R. Zhang, “3d localization of weak scatterers in digital holographic microscopy using rayleigh-sommerfeld back-propagation”, *Optics Express* **20**, 16735 (2012).
- [62] J. W. Goodman, *Introduction to fourier optics*, Google-Books-ID: ow5xs\_Rtt9AC (Roberts and Company Publishers, 2005), 520 pp.
- [63] F. C. Cheong, B. J. Krishnatreya, and D. G. Grier, “Strategies for three-dimensional particle tracking with holographic video microscopy”, *Optics Express* **18**, Publisher: Optical Society of America, 13563–13573 (2010).
- [64] G. C. Sherman, “Application of the convolution theorem to rayleigh’s integral formulas”, *JOSA* **57**, Publisher: Optical Society of America, 546–547 (1967).
- [65] U. Schnars and W. P. Jüptner, “Digital recording and reconstruction of holograms in hologram interferometry and shearography”, *Applied Optics* **33**, 4373–4377 (1994).
- [66] T. M. Kreis, “Frequency analysis of digital holography with reconstruction by convolution”, *Optical Engineering* **41**, Publisher: International Society for Optics and Photonics, 1829–1839 (2002).
- [67] J. J. Moré, “The levenberg-marquardt algorithm: implementation and theory”, in Numerical analysis, edited by G. A. Watson, Lecture Notes in Mathematics (1978), pp. 105–116.
- [68] J. N. Israelachvili, *Intermolecular and surface forces*, Google-Books-ID: MVbWB-hubrgIC (Academic Press, May 29, 2015), 706 pp.
- [69] G. M. Bell, S. Levine, and L. N. McCartney, “Approximate methods of determining the double-layer free energy of interaction between two charged colloidal spheres”, *Journal of Colloid and Interface Science* **33**, 335–359 (1970).

- [70] S. H. Behrens and D. G. Grier, “The charge of glass and silica surfaces”, *The Journal of Chemical Physics* **115**, 6716–6721 (2001).
- [71] J. Gregory, “Approximate expressions for retarded van der waals interaction”, *Journal of Colloid and Interface Science* **83**, 138–145 (1981).
- [72] H. Brenner, “The slow motion of a sphere through a viscous fluid towards a plane surface”, *Chemical Engineering Science* **16**, 242–251 (1961).
- [73] H. Faxen, “Fredholm integral equations of hydrodynamics of liquids i”, *Ark. Mat., Astron. Fys* **18**, 29–32 (1924).
- [74] A. J. Goldman, R. G. Cox, and H. Brenner, “Slow viscous motion of a sphere parallel to a plane wall—i motion through a quiescent fluid”, *Chemical Engineering Science* **22**, 637–651 (1967).